F. Merkt and H. J. Wörner

DOI: 10.1002/anie.200900526

Molecular Spectroscopy

Jahn–Teller Effects in Molecular Cations Studied by Photoelectron Spectroscopy and Group Theory

*Hans Jakob Wörner and Frédéric Merkt**

Keywords:
ab initio calculations · fluxionality · isomerization · Jahn–Teller effect · photoelectron spectroscopy

Dedicated to Professor Martin Quack on the occasion of his 60th birthday

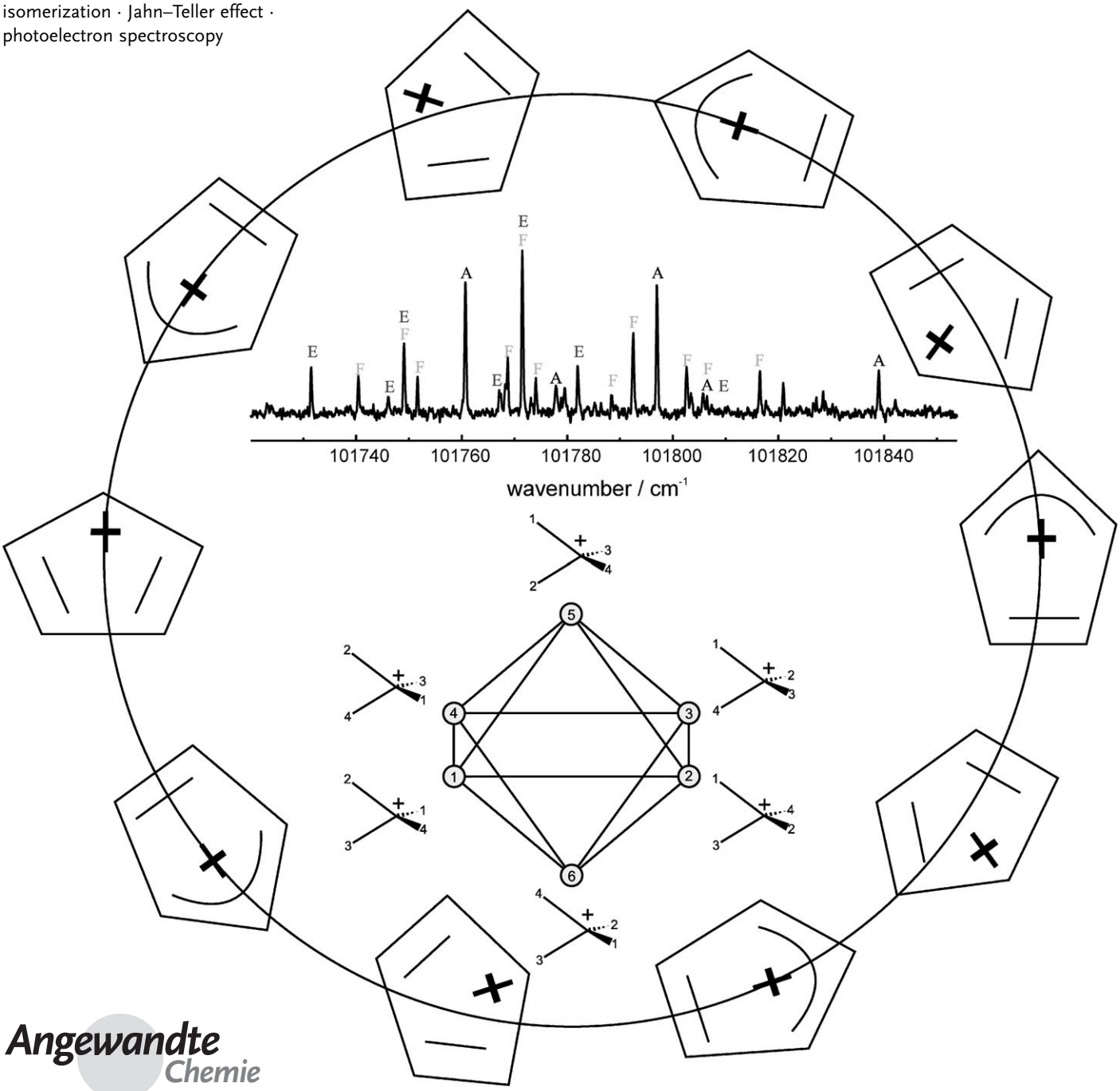

The traditional "ball-and-stick" concept of molecular structure fails when the motion of the electrons is coupled to that of the nuclei. Such a situation arises in the Jahn–Teller (JT) effect which is very common in open-shell molecular systems, such as radicals or ions. The JT effect is well known to chemists as a mechanism that causes the distortion of an otherwise symmetric system. Its implications on the dynamics of molecules still represent unsolved problems in many cases. Herein we review recent progress in understanding the dynamic structure of molecular cations that have a high permutational symmetry by using rotationally resolved photoelectron spectroscopy and group theory. Specifically, we show how the pseudo-Jahn–Teller effect in the cyclopentadienyl cation causes electronic localization and nuclear delocalization. The fundamental physical mechanisms underlying the vaguely defined concept of "antiaromaticity" are thereby elucidated. Our investigation of the methane cation represents the first experimental characterization of the JT effect in a threefold degenerate electronic state. A special kind of isomerism resulting from the JT effect has been discovered and is predicted to exist in all JT systems in which the minima on the potential-energy surface are separated by substantial barriers.

From the Contents

1. Introduction

The Jahn–Teller (JT) and pseudo-Jahn–Teller (PJT) effects arise from the coupling of electronic and nuclear degrees of freedom in systems with degenerate or near-degenerate states and influences the structural and dynamic properties of molecules, transition-metal complexes, and solids. The variety of its physical and chemical implications is extremely rich.[1,2]

In electronically degenerate states of molecules and transition-metal complexes, the JT effect lowers the potential energy for configurations in which the arrangement of the nuclei has a reduced symmetry. If the corresponding JT stabilization energy is large compared to the vibrational energy intervals, the JT effect results in a distortion of the molecule. In organic molecules, the JT effect is essential in the interpretation of photochemistry and in the definition of antiaromaticity. In solids, the JT effect has been invoked to explain phenomena such as superconductivity and colossal magnetoresistance.[1] The JT effect occurs in species with unpaired electrons, in particular, radicals and biradicals. Such molecules are usually highly reactive and play an important role as reaction intermediates, in combustion chemistry, atmospheric chemistry, and the chemistry of the interstellar medium.

The first advances in the investigation of the JT effect were of a theoretical nature. Hermann Jahn and Edward Teller used group theory to demonstrate that a nonlinear molecule in an orbitally degenerate state undergoes a geometric distortion.[3,4] Longuet-Higgins et al.[5,6] calculated the vibronic energy-level structure resulting from the interaction of a doubly degenerate electronic state (E) with one doubly degenerate vibrational mode (e), which is called the E⊗e JT effect. They predicted the band shapes of optical absorption spectra and pointed at the first observable manifestations of the JT effect in optical spectra. A molecule subject to a JT effect can distort along several equivalent vibrational modes giving rise to equivalent minima on the potential-energy surface. Bersuker recognized that this situation leads (in most cases) to a splitting of the lowest vibronic levels by tunneling.[7] Öpik and Pryce investigated the interaction of triply degenerate electronic states (T) and doubly (e) and triply (t) degenerate vibrational modes in molecules of the cubic point groups, which is known as the T⊗(e+t_2) effect and considered for the first time the vibronic coupling between nondegenerate electronic states, also called the pseudo-Jahn–Teller (PJT) effect.[8]

The most detailed experimental characterization of the JT effect has been achieved by high-resolution optical and photoelectron spectroscopy. Optical spectroscopy has been applied to elucidate the JT effect in several open-shell species including Na_3 and Li_3. The $\tilde{A}\,^2E''$ state of these species represents the prototype of the E⊗e JT effect.[9] The next higher electronic state $\tilde{B}\,^2A'_1$ is subject to a PJT effect.[10,11] Photoelectron spectroscopy has been used to characterize the JT effect in a wide range of molecular cations. For instance, the analysis of rotationally resolved PFI-ZEKE photoelectron spectra of C_6H_6 has demonstrated that the minima of the ground-state potential-energy surface of $C_6H_6^+$, which is subject to the E⊗e JT effect, correspond to a D_{2h} geometry with two acute C-C-C bond angles, although the rovibronic photoionization selection rules are adequately described in D_{6h}(M) symmetry.[12,13]

[*] Dr. H. J. Wörner, Prof. Dr. F. Merkt
Laboratorium für Physikalische Chemie, ETH-Zürich
8093 Zürich (Switzerland)
E-mail: frederic.merkt@ethz.ch

Currently, the E⊗e JT effect is the best understood case and its ramifications are well known.[1,14–18] Much less is known about other cases, especially about molecules of higher symmetry, in which the electronic states can have threefold or higher degeneracies.[19] This lack of information is primarily because of the scarcity of high-resolution spectroscopic data that would permit the determination of the structure and dynamics of such species.

Herein we focus on recent experimental and theoretical progress in understanding the JT effect in highly symmetrical molecules. We demonstrate how rotationally resolved photoelectron spectroscopy permits the investigation of molecular cations that, as a consequence of the JT or PJT effects, are highly fluxional in their ground electronic state. In this Review we also introduce a group theoretical formalism that enables the assignment and interpretation of the experimental results.

The experiments rely on the combination of pulsed-field-ionization zero-kinetic-energy (PFI-ZEKE) photoelectron spectroscopy[20,21] with double-resonance excitation schemes involving mid-infrared, visible, and ultraviolet radiation. These developments were essential in assigning the complex spectra because, initially, no theoretical framework existed that could have guided the assignment procedure. A theoretically methodology has now been developed to predict the rovibronic symmetry labels for the observed transitions of the molecules undergoing the JT effect. The method makes use of ab initio quantum chemical calculations and of the complete nuclear permutation inversion (CNPI) or the molecular symmetry (MS) groups[22] that are adequate for describing highly fluxional systems. The ab initio calculations are used to predict the minimum energy structures. Symmetry correlations between the CNPI or the MS group and the point group of the distorted minimum structures are used to predict all rovibronic levels, including their symmetry label.

For this Review, the systems we have chosen are the methane cation, which was the first example of the JT effect in a triply degenerate electronic state characterized at the level of the rotational structure, and the cyclopentadienyl cation as it is a prototypical molecule with which to study the interplay of the PJT effect and antiaromaticity. The methane cation is one of the simplest systems subject to a T⊗(e+t_2) JT effect and the cyclopentadienyl cation displays properties influenced by a complex interplay of PJT and JT effects. These two radical cations are of fundamental importance in chemistry and molecular physics but neither of them had been characterized in sufficient detail to obtain definitive structural and dynamic information, prior to the work described herein. The reason for this situation lies in the difficulty in producing these charged species in sufficient quantities to allow a spectroscopic investigation at high resolution.

Section 2 summarizes the theoretical methods used to describe the JT and PJT effects, with emphasis on group theory and its applications to the methane cation and the cyclopentadienyl cation. Section 3 describes the experimental methods, in particular the double-resonance excitation schemes used in the assignment of the rovibronic structure of photoelectron spectra. In Section 4, the general energy-level structures of CH_4^+ and $C_5H_5^+$ are described and interpreted. Section 5 is dedicated to two phenomena arising in some isotopically substituted molecules as a consequence of the JT effect: isomerism and chirality. Section 6 presents the applicability of the group-theoretical method to other systems that are not subject to a JT effect. The last section consists of a short summary and an outlook.

2. Theoretical Considerations

2.1. Vibronic Coupling and Molecular Symmetry

Neglecting spins and molecular rotations, the Hamiltonian of a polyatomic molecule can be written as Equation (1).

$$\hat{H} = \hat{H}_{\mathrm{el.}}(\vec{r}) + \hat{H}_{\mathrm{nuc.}}(\vec{Q}) + \hat{V}(\vec{r},\vec{Q}) \quad (1)$$

$\hat{H}_{\mathrm{el.}}(\vec{r})$ is the electronic part of the operator including the kinetic energy of the electrons and their electrostatic interactions, $\hat{H}_{\mathrm{nuc.}}(\vec{Q})$ is the kinetic energy operator of the nuclei and $\hat{V}(\vec{r},\vec{Q})$ is the potential energy operator representing the interaction of the electrons and the nuclei and the internu-

Hans Jakob Wörner was born in Freiburg (Germany) in 1981, studied chemistry at EPF Lausanne and ETH Zurich (2003). In 2007 he completed his Ph.D. thesis under the guidance of Prof. F. Merkt on high-resolution photoionization and photoelectron spectroscopy focused on non-Born–Oppenheimer effects in molecular cations. For his thesis he was awarded the ETH medal for outstanding dissertations. He then was a postdoctoral researcher in the group of Dr. Ch. Jungen at the Université de Paris-Sud, Orsay (theoretical description of molecular Rydberg states). In 2007 he joined the group of Prof. P. Corkum at NRC in Ottawa, Canada, where he works since on new spectroscopic methods with attosecond time resolution.

Frédéric Merkt received his degree in chemistry in 1988 from ETH Zurich and his Ph.D. in 1992 from Cambridge University, (England), under the guidance of Prof. T. P. Softley on the generation and spectroscopic application of VUV laser radiation. He was as a postdoctoral researcher in the group of Dr. P. M. Guyon at the Université de Paris-Sud, Orsay (1992) and in the group of Prof. R. N. Zare at Stanford University (1993–1994). He then worked at Oxford University where he held a junior research fellowship at St. John's College before returning to ETH Zurich as assistant professor in 1995. He has been full Professor of Physical Chemistry there since 1999. He has received the Swiss National Latsis Prize and the Alfred Werner Prize of the Swiss Chemical Society (1999) and the Akademiepreis der Berlin-Brandenburgischen Akademie der Wissenschaften (2004).

clear repulsion. In standard treatments of the JT effect (see Refs. [1,2,17,23]), $\hat{V}(\vec{r},\vec{Q})$ is expanded in a Taylor series of small displacements of the nuclei about a reference geometry $\vec{Q}_0$ of highest symmetry [Eq. (2)] where Q_i represents the symmetrized displacement coordinates (or vibrational modes). In Equation (2), and throughout this Review, we neglect the contributions of terms containing mixed derivatives in two or more coordinates (so-called bilinear and higher-order coupling terms).

$$\hat{V}(\vec{r},\vec{Q}) = \sum_{k=0}^{\infty} \frac{1}{k!} \sum_{i=1}^{3N-6} \left(\frac{\partial^k \hat{V}}{\partial Q_i^k} \right)_0 Q_i^k \tag{2}$$

Retaining only the first term of the Taylor series $\hat{V}(\vec{r},\vec{Q}^0)$, the electronic part of the Schrödinger equation can be solved with fixed nuclei at the reference geometry [Eq. (3)] giving a set of energies ε_i' and so-called diabatic electronic wave functions $|\phi_i(\vec{r})\rangle$.

$$\left[\hat{H}_{\text{el.}} + \hat{V}(\vec{r},\vec{Q}^0)\right] |\phi_i(\vec{r})\rangle = \varepsilon_i' |\phi_i(\vec{r})\rangle \tag{3}$$

The general solution of the Schrödinger equation for moving nuclei can be expanded in terms of the electronic functions [Eq. (4)] where the expansion coefficients $\chi_i(\vec{Q})$ are functions of the nuclear coordinates.

$$\Psi(\vec{r},\vec{Q}) = \sum_i \chi_i(\vec{Q}) |\phi_i(\vec{r})\rangle \tag{4}$$

Expressing the Schrödinger equation corresponding to the Hamiltonian in Equation (1) in the basis of the diabatic electronic wave functions $|\phi_i(\vec{r})\rangle$ provides a system of coupled equations [Eq. (5)] in which W_{ij} are the elements of the vibronic interaction matrix [Eq. (6)][1] and $\varepsilon_i(\vec{Q})'$ is the eigenenergy of the diabatic electronic wave function defined in Equation (3) at the arbitrary geometry $\vec{Q}$.

$$\left[\hat{H}_{\text{nuc.}} + \varepsilon_i(\vec{Q})' + W_{ii}(\vec{Q})\right] \chi_i(\vec{Q}) + \sum_{j \neq i} W_{ij} \chi_i(\vec{Q}) = E \chi_i(\vec{Q}), \tag{5}$$

$$W(\vec{r},\vec{Q}) = V(\vec{r},\vec{Q}) - V(\vec{r},\vec{Q}^0) \tag{6}$$

If the vibronic interactions can be neglected, the coupled Equations (5) decompose into a set of simple equations that can be solved independently for each electronic state, which is known as the Born–Oppenheimer (BO) approximation. If the vibronic interactions cannot be neglected, a separation is not possible and the coupled Equations (5) must be solved together.

The solution of a particular vibronic coupling problem is considerably simplified by exploiting the molecular symmetry. The operators in Equation (3) and, in particular, the potential-energy operator in Equation (2) are invariant under all operations of the complete nuclear permutation inversion (CNPI) group or molecular symmetry group of the molecule.[22] A nonvanishing contribution to vibronic coupling between the electronic states of irreducible representations Γ_A and Γ_B only exists for a term of order k in Equation (2) if the relationship in Equation (7) holds.

$$\Gamma_A \otimes \Gamma_B \supseteq [\Gamma_\nu]^k \tag{7}$$

$[\Gamma_\nu]^k$ is the symmetric k^{th} power of the irreducible representation of the vibrational mode ν. The corresponding vibration is then called "active". Vibronic coupling between the different components of a degenerate electronic state of irreducible representation $\Gamma_{\text{el,deg.}}$, which is known as the Jahn–Teller effect, is allowed along mode ν if the conditions in Equation (8) are met.

$$\left[\Gamma_{el,deg.}\right]^2 \supseteq [\Gamma_\nu]^k \tag{8}$$

The coupling between a degenerate state ($\Gamma_{\text{el,deg.}}$) and a nondegenerate state ($\Gamma_{\text{el,nondeg.}}$), the so-called pseudo-Jahn–Teller effect, can only occur along mode ν if the conditions in Equation (9) are met.

$$\Gamma_{el,deg.} \otimes \Gamma_{el,nondeg.} \supseteq [\Gamma_\nu]^k \tag{9}$$

After identification of the JT and PJT active modes, the vibronic Hamiltonian is set up in the basis of diabatic electronic states defined in Equation (3). The active modes are designated by their irreducible representation Γ_ν which has several components γ if the representation is degenerate. The kinetic energy term of the nuclear Hamiltonian can be expressed as Equation (10) where μ_ν is the reduced mass of the vibrational mode.

$$\hat{H}_{\text{kin}} = \sum_{\nu_\gamma} -\frac{\hbar^2}{2\mu_\nu} \frac{\partial^2}{\partial Q_{\nu_\gamma}^2} \mathbf{1} \tag{10}$$

The potential energy term, truncated to second order, is given by Equation (11) where V_ν and K_ν are the linear and quadratic coupling constants and ω_ν is the vibrational frequency of the vibrational mode ν. $\mathbf{C}_{\nu_\gamma}$ is a matrix of Clebsch–Gordan coefficients that can be found in tables in the literature.[24,25]

$$V(\vec{Q}) = \sum_{\nu_\gamma} \left(\frac{1}{2} \mu_\nu \omega_\nu^2 Q_{\nu_\gamma}^2 \mathbf{1} + V_\nu Q_{\nu_\gamma} \mathbf{C}_{\nu_\gamma} + K_\nu Q_{\nu_\gamma}^2 \mathbf{1} \right) \tag{11}$$

Adiabatic potential energy surfaces $E(\vec{Q})$ and electronic state vectors $\left|a(\vec{Q})\right\rangle$ are obtained by solving Equation (12).

$$V(\vec{Q}) \left|a(\vec{Q})\right\rangle = E(\vec{Q}) \left|a(\vec{Q})\right\rangle \tag{12}$$

These quantities provide a simple picture of the vibronic coupling problem that reveals its essential aspects of symmetry and topology.

The comparison with observed energy levels requires solving the coupled electronic–vibrational problem, which is in general very difficult. The traditional approach consists of representing the problem in a direct product basis of diabatic electronic functions and harmonic oscillator functions of the appropriate degeneracy and subsequently diagonalizing the matrices.[5,15,17] The vibrational basis is increased until convergence is reached. The size of the matrices grows very quickly with the magnitude of the Jahn–Teller stabilization energy and the number of vibrational modes involved. In

spite of efficient iterative diagonalization algorithms (e.g., the Lanczos algorithm[26]), only a small number of modes can be treated simultaneously if the stabilization energy is large. This procedure is applied below to the analysis of the spectra of the cyclopentadienyl cation. The lowest singlet state is subject to a PJT stabilization of approximately 5000 cm^{-1} involving four doubly degenerate modes. In the case of the methane cation, which undergoes a JT stabilization of approximately 12000 cm^{-1} mediated by two triply and one doubly degenerate modes, the solution of the coupled problem is a tremendous task, and we therefore opted for a simplified approach based on an effective Hamiltonian and exploiting the molecular symmetry.

2.2. The Role of Ab Initio Calculations in the Elucidation of JT Problems

Traditional ab initio quantum chemical calculations are performed at a frozen configuration of the nuclei according to Equation (3) using the Born–Oppenheimer (BO) approximation. Since the JT effect results from the coupling between nuclear and electronic degrees of freedom, which implies a failure of the BO approximation, questioning the utility of ab initio calculations according to Equation (3) in understanding JT problems is justified.

Ab initio calculations are capable of predicting the minimum energy geometry and the amount of electronic potential energy by which a molecule is stabilized compared to the geometry of highest symmetry where two or more electronic states are degenerate (the so-called JT stabilization energy). These parameters, as well as the intersections of electronic-potential surfaces are nowadays accessible by specialized methods of ab initio calculation and the JT coupling parameters can be efficiently predicted (see, e.g. Ref. [27]). These data are essential parameters to describe the JT effect in a molecule, but are in general insufficient to predict the coupled nuclear and electronic dynamics and the rovibronic energy-level structure of a molecule. Indeed, in molecules with a high permutational symmetry, the JT effect leads to several equivalent minima on the potential-energy surface. If these minima are connected by low energy barriers, large-amplitude motions take place giving rise to complex energy-level structures. Herein, we illustrate the use of ab initio calculations to predict the molecular geometry at the minima of the potential-energy surface and the use of group theory to predict the resulting rovibronic quantum states.

The most accurate solution of the coupled electronic–vibrational problem is given by the formalism outlined in Section 2.1. It provides the complete solution of the vibronic problem for arbitrary energies, including regions where electronic surfaces intersect and the BO approximation breaks down. In cases like that of the methane cation which has a JT stabilization energy of approximately 1.5 eV, this procedure is too demanding and a simpler solution is needed. Indeed, when the JT stabilization energy is large, the BO approximation provides an accurate description of the nuclear dynamics in the region of the potential-energy minima. However, one essential aspect needs consideration. The adiabatic electronic wave function changes its character from one equivalent minimum to another. This property can be described by a geometric (or topological) phase[28] which affects the energy-level structure of JT systems. In the case of the E⊗e JT effect, the geometric phase reverses the energetic ordering of vibronic levels from A below E to E below A.[9] In the $T_2\otimes(e+t_2)$ case, it even changes the symmetry of vibronic levels from A, F_2, E to F_2, F_1.[*][29]

2.3. Jahn–Teller Effects in Diradicals of Configuration e^2

Diradicals which have two electrons in a degenerate orbital form an important class of molecules which encompasses the so-called "antiaromatic" molecules, the simplest of which are the cyclopropenyl anion, cyclobutadiene, and the cyclopentadienyl cation. In the following, we briefly formulate the vibronic coupling theory describing these systems, emphasizing the simplifications arising from symmetry considerations. The left-hand side of Figure 1 displays the

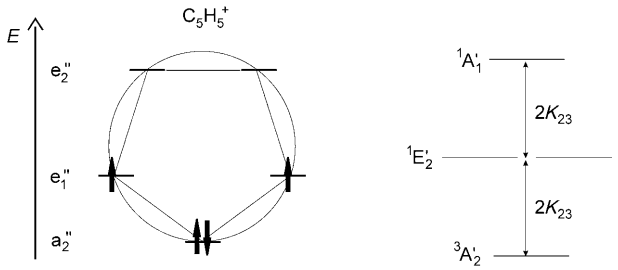

Figure 1. Left: Frost–Musulin diagram of the lowest-lying electronic configuration of the cyclopentadienyl cation. Right: energetic ordering of the corresponding electronic states in D_{5h} symmetry. K_{23} represents the exchange integral (see text; Figure adapted from Ref. [34]).

energetic ordering of the a_2'', e_1'', and e_2''molecular orbitals of $C_5H_5^+$ in the form of a Frost–Musulin diagram. In the D_{nh}(M) symmetry groups in which n is odd, the ground configuration $(a_2'')^2(e_1'')^2$ gives rise to the three states $^3A_2'$, $^1E_2'$, and $^1A_1'$ displayed on the right-hand side of Figure 1. The Hartree–Fock energies of these three states are $2h+J_{23}-K_{23}$, $2h+J_{23}+K_{23}$, and $2h+J_{22}+K_{23}$, respectively, where h, J_{ij}, and K_{ij} represent the one-electron orbital energy, the Coulomb integral, and the exchange integral, respectively, and the indices designate the π molecular orbitals in order of increasing energy[30] (by symmetry $J_{22}-J_{23}=2K_{23}$).

Neglecting spin–orbit interactions and coupling with higher-lying triplet states, the $^3A_2'$ ground electronic state of $C_5H_5^+$ does not undergo vibronic coupling. The lowest-lying singlet state $^1E_2'$ is degenerate and, in this state, the e_1' modes induce a linear JT effect and the e_2' and e_2'' modes induce a

[*] The commonly used label for the JTE still employs the letters T or t to designate triply degenerate electronic states and vibrational modes, respectively, rather than the recommended F and f labels used in the remainder of this Review.

quadratic JT effect. The e'_2 modes also induce a linear PJT coupling between the $^1E'_2$ and the $^1A'_1$ states. These results and those for higher-order vibonic interactions are summarized in Table 1.

Table 1: Vibrational symmetries of Jahn–Teller active modes in a state of electronic symmetry E'_2 and pseudo-Jahn–Teller active modes coupling a state of electronic symmetry E'_2 with a state of symmetry A'_1 for a molecule of symmetry D_{5h}(M) up to third order.

JT activity in E'_2		PJT activity $E'_2 \leftrightarrow A'_1$	
Order	Γ_{vib}	Order	Γ_{vib}
1	e'_1	1	e'_2
2	e'_2, e''_2	2	e'_1, e''_1
3	e'_1, e'_2	3	e'_1, e'_2

The coupled Hamiltonian is most conveniently set up in a diabatic electronic basis. Using complex basis functions for the E state and retaining only linear coupling terms, the Hamiltonian H can be written in matrix form as Equation (13)[31] where H^{PJT} and H^{JT} are given by Equations (14) and (15), respectively.

$$H = H^{PJT} + H^{JT} \tag{13}$$

$$H^{PJT} = h_0^{PJT}\mathbf{1} + \begin{pmatrix} E_E & 0 & \sum_j \lambda_j r_j e^{i\phi_j} \\ 0 & E_E & \sum_j \lambda_j r_j e^{-i\phi_j} \\ \text{H.c.} & \text{H.c.} & E_A \end{pmatrix} \tag{14}$$

$$H^{JT} = h_0^{JT}\mathbf{1} + \begin{pmatrix} 0 & \sum_n g_n \rho_n e^{-i\theta_n} & 0 \\ \text{H.c.} & 0 & 0 \\ 0 & 0 & 0 \end{pmatrix} \tag{15}$$

The degenerate vibrational modes mediating the vibronic coupling are described by cylindrical mass-weighted dimensionless normal coordinates r_j, ϕ_j, and ρ_n, θ_n, which are related to the Cartesian coordinates x_j and y_j (x_n and y_n) as indicated in Figures 2 and 3. The first and second terms in Equation (13) represent the PJT and JT interactions, respectively (H.c. means "Hermitian conjugate"), with linear coupling constants λ_j and g_n, respectively. The indices j and n label the PJT and JT active modes, respectively. The harmonic oscillator terms h_0^{PJT} und h_0^{JT} in Equations (14) and (15) take the form of Equations (16) and (17), respectively.

$$h_0^{PJT} = \sum_j \frac{\omega_j}{2}\left(-\frac{1}{r_j}\frac{\partial}{\partial r_j} r_j \frac{\partial}{\partial r_j} - \frac{1}{r_j^2}\frac{\partial^2}{\partial \phi_j^2} + r_j^2\right) \tag{16}$$

$$h_0^{JT} = \sum_n \frac{\omega_n}{2}\left(-\frac{1}{\rho_n}\frac{\partial}{\partial \rho_n} \rho_n \frac{\partial}{\partial \rho_n} - \frac{1}{\rho_n^2}\frac{\partial^2}{\partial \theta_n^2} + \rho_n^2\right) \tag{17}$$

The adiabatic potential-energy surfaces have a simple appearance when only either JT or PJT displacements are considered. In the case of a single JT-active mode with cylindrical coordinates (ρ,θ) a characteristic potential is obtained for the E state [Eq. (18)] as represented in Figure 2.

$$V_{E^\pm}(\rho,\theta) = V_{E^\pm}(\rho) = V_E(0) + \frac{\omega_{JT}}{2}\rho^2 \pm g\rho \tag{18}$$

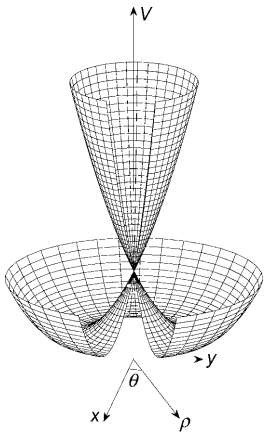

Figure 2. Adiabatic potential-energy surfaces resulting from a linear Jahn–Teller effect in a doubly degenerate electronic state induced by a single, doubly degenerate vibrational mode [see Eq. (18)]. The parameters used are $\omega_{JT} = 800\ cm^{-1}$ and $g = 500\ cm^{-1}$.

For a single PJT-active mode with cylindrical coordinates (r,ϕ), two of the surfaces repel each other whereas the third remains unchanged. Assuming identical vibrational frequencies in the A and E states, the potential surfaces described by Equations (19a–c) are obtained as represented in Figure 3.

$$V_A(r,\phi) = V_A(r) = \frac{V_E(0) + V_A(0)}{2} + \frac{\omega_{PJT}}{2}r^2 + \sqrt{\left[\frac{V_A(0) - V_E(0)}{2}\right]^2 + 2\lambda^2 r^2} \tag{19a}$$

$$V_{E_y}(r,\phi) = V_{E_y}(r) = V_E(0) + \frac{\omega_{PJT}}{2}r^2 \tag{19b}$$

$$V_{E_x}(r,\phi) = V_{E_x}(r) = \frac{V_E(0) + V_A(0)}{2} + \frac{\omega_{PJT}}{2}r^2 - \sqrt{\left[\frac{V_A(0) - V_E(0)}{2}\right]^2 + 2\lambda^2 r^2} \tag{19c}$$

Both the JT and PJT interactions lift the electronic degeneracy in the $^1E'_2$ state but the effects are qualitatively different as can be seen in Figure 4. Both e'_1 and e'_2 modes have

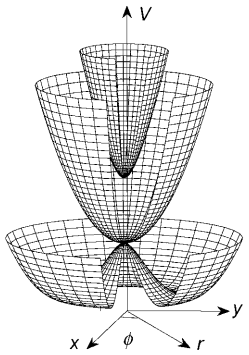

Figure 3. Adiabatic potential-energy surfaces resulting from a linear pseudo-Jahn–Teller effect between a lower lying, doubly degenerate electronic state (E) and a higher lying, nondegenerate state (A) induced by a single, doubly degenerate vibrational mode [see Eq. (19a–c)]. The parameters used are $\omega_{PJT} = 800\ cm^{-1}$, $V_A(0) - V_E(0) = 5600\ cm^{-1}$ and $\lambda = 2400\ cm^{-1}$.

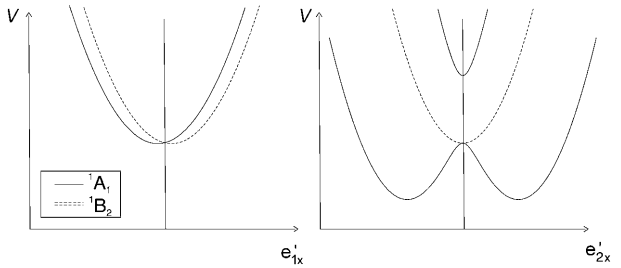

Figure 4. Adiabatic potential-energy surfaces arising from the linear Jahn–Teller effect (left) and the pseudo-Jahn–Teller effect in the $^1E'_2$ and $^1A'_1$ states (right). The axes are chosen to be the *x* components of the effective e'_1 and e'_2 modes that connect the D_{5h} geometry point (indicated by the vertical line) to the respective minima. Both modes preserve C_{2v} symmetry which enables the attribution of electronic symmetries to each curve. Electronic symmetries in the D_{5h} group are given corresponding to the cyclopentadienyl cation.

two components e'_x and e'_y. A distortion along an e'_x component conserves C_{2v} symmetry, whereas a distortion along an e'_y component lowers the symmetry to C_s. A distortion from D_{5h} to C_{2v} symmetry splits the $^1E'_2$ state into two components of symmetry $^1A_1$ and $^1B_2$ (full and dashed lines, respectively in Figure 4). In the case of a linear JT effect, the potential-energy surfaces have a nonzero slope at the point of D_{5h} symmetry and, consequently, their ordering is reversed when the sign of the distortion coordinate is changed. In the case of a quadratic JT or a PJT effect, the slope of the adiabatic electronic surfaces vanishes at the point of highest symmetry and the ordering of the two components is independent of the sign of the distortion coordinate. In the present case, the lower component is totally symmetric ($^1A_1$ in C_{2v}) whereas the upper component has symmetry $^1B_2$ in C_{2v}.

The linear JT effect in an electronic state having two electrons in two degenerate orbitals (configuration e^2) vanishes if configuration interaction is neglected.[32] The coupling constants of the three e'_1 modes in the $^1E'_2$ state are indeed found to be very small.[33,34] The linear PJT effect in the four modes of symmetry e'_2 on the contrary is very strong and leads to a deep minimum energy trough on the lowest potential-energy surface as shown in Figure 3. The distortion of the molecule changes continuously along the minimum of the surface, as shown in Figure 5a. Figure 5b illustrates the geometric and electronic structure of the molecule if the distortion follows an e'_{2x} distortion from the reference geometry to the two minima. A remarkable property is the absence of quadratic PJT coupling in the e'_2 modes which is imposed by the molecular symmetry (see Table 1) and implies that pseudorotation along the circular minimum-energy path in Figure 3 (which corresponds to the circle depicted in Figure 5a) is unhindered. The vibronic singlet ground-state wave function of the cyclopentadienyl cation is thus completely delocalized over the pseudorotation path.

2.4. The Jahn–Teller Effect in a Triply Degenerate Electronic State

Threefold degenerate electronic states are common in highly symmetric molecules with unpaired electrons such as

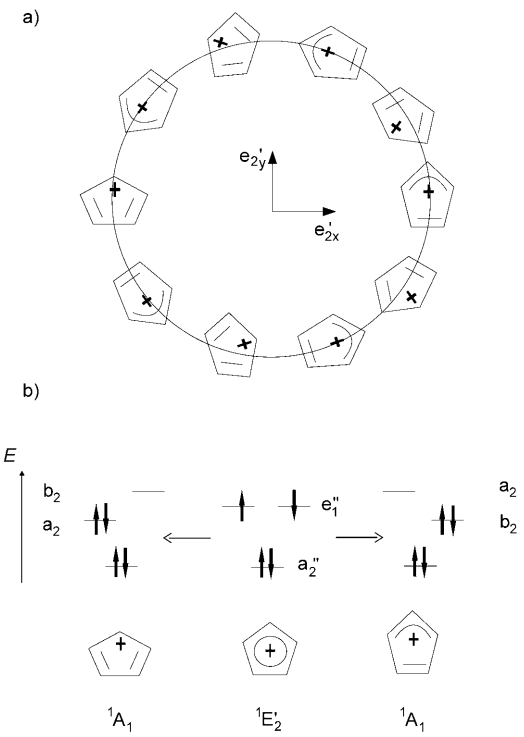

Figure 5. a) Schematic representation of the minimum energy pseudorotation path in the lowest singlet state. A distortion along the e'_{2x} dimension preserves C_{2v} symmetry and takes the molecule to either the allylic or dienylic structure. If vibronic coupling terms of third and higher orders are neglected, the minimum energy path displayed is isoenergetic. b) Electronic configurations of the $\tilde{a}^{+\,1}E'_2$ state at D_{5h} symmetry (middle) and of the distorted dienylic and allylic structures (left and right, respectively). The ordering of the a_2 and b_1 molecular orbitals originating from the degenerate e''_1 orbital is opposite in the dienylic and allylic structures (adapted from Ref. [34]).

CH_4^+ or P_4^+ and especially also in transition-metal complexes. The JT problem resulting from the configuration t^1 (or t^5) is very rich and has been studied theoretically in, for example, Ref. [24]. In a triply degenerate electronic state, the twofold and threefold degenerate vibrational modes (e and f) are JT active (Table 2). Distortion along a mode of vibrational symmetry e leads to a minimum-energy geometry of tetragonal symmetry, whereas distortion along an f mode results in a trigonal minimum geometry. If JT activity is limited to the linear term, these are the only possible minima, even when both modes are simultaneously active.

Only when quadratic JT activity is permitted does a new kind of minima appear, which is of lower symmetry. This case,

Table 2: Vibrational symmetries of Jahn–Teller active modes in a state of electronic symmetry F_2 for a molecule of symmetry T_d(M) up to third order.

	JT activity in F_2
Order	Γ_{vib}
1	e, f_2
2	e, f_2
3	e, f_2

which applies to the methane cation, is illustrated in Figure 6 and Figure 7. The tetrahedral configuration corresponds to a triply degenerate conical intersection. If the molecule is distorted along the two vibrational modes of symmetry f_2 it

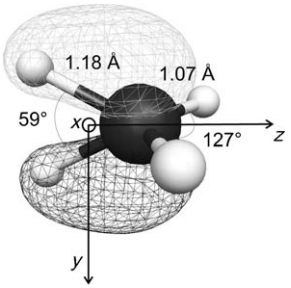

Figure 6. Equilibrium geometry of the CH_4^+ ion, structure of its highest lying, singly occupied molecular orbital at the global minimum of the potential-energy surface at the UMP2/cc-pVDZ level of ab initio theory and principal axes of inertia. The structure has C_{2v} geometry and the H-C-H bond angles and C–H bond lengths are indicated.

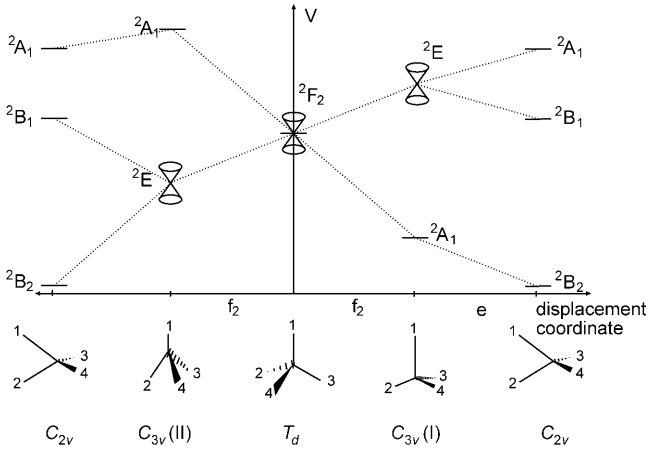

Figure 7. Schematic representation of the three potential-energy surfaces of the methane cation arising from the Jahn–Teller effect in its $^2F_2$ ground state. The vertical axis represents the electronic potential energy, the horizontal axis represents effective displacement coordinates, the symmetries of which are indicated. The structures corresponding to the represented stationary points and their point group are indicated below the graph.

can reach either the structure C_{3v}(II) or the structure C_{3v}(I) depicted in Figure 7. The C_{3v}(II) structure has one short and three long C–H bonds, and has a doubly degenerate ground state (^2E in C_{3v}(M)) corresponding to a twofold conical intersection and a nondegenerate first excited state ($^2A_1$ in C_{3v}(M)). The C_{3v}(I) structure has one long and three short C–H bonds and has a nondegenerate ground electronic state ($^2A_1$ in C_{3v}(M)) and a doubly degenerate first excited electronic state (^2E in C_{3v}(M)). Further distortions along the e modes lead to the C_{2v} minimum-energy structure depicted in Figure 6 and which is characterized by two long C–H bonds separated by a small angle (ca. 60°) and two short C–H bonds separated by a large angle (ca. 127°).

The total stabilization energy amounts to about 12000 cm^{-1}.[35–37] The number of equivalent structures of a given symmetry is determined by the ratio of the order of the CNPI group of the molecule and the order of the point group of the structure. The CNPI of CH_4^+ has order 48 and therefore there are eight equivalent structures of each of the two C_{3v} geometries displayed in Figure 7. For the D_{2d} geometry there are six equivalent structures and 12 for the C_{2v} geometry. The 12 possible C_{2v} structures fall in two sets of six structures, each of which are mirror images of each other.[35] One of these sets is represented in Figure 8 along with the adiabatic electronic

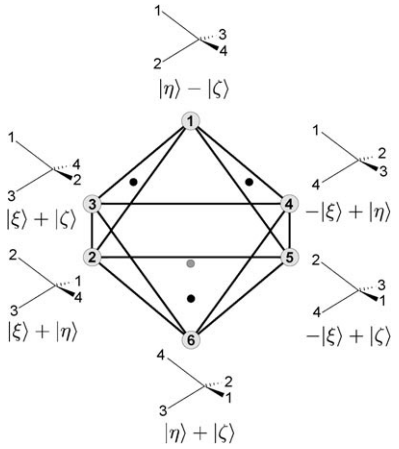

Figure 8. Topological representation of the connectivity of the six equivalent minimum-energy structures of C_{2v} symmetry of CH_4^+. The vertices correspond to the C_{2v} minimum-energy geometries and the edges to the equivalent pseudorotation–tunneling paths connecting the minima via low-lying C_s transition states. Four faces of the octahedron correspond to a C_{3v} geometry with a degenerate ground state (structure C_{3v}(II) of Figure 7, marked with a dot) and the other four faces correspond to a C_{3v} geometry with a nondegenerate ground state (structure C_{3v}(I) of Figure 7). The adiabatic electronic wavefunction $|n\rangle$ is indicated below each structure as a linear combination of the three diabatic basis functions ($|\xi\rangle$, $|\eta\rangle$, $|\zeta\rangle$) defined at the T_d geometry.

function corresponding to the local minimum expressed as linear combination of the three diabatic electronic functions $|\eta\rangle$, $|\xi\rangle$, and $|\zeta\rangle$. The very large stabilization energy and the eight-dimensional space of JT active vibrations render a complete vibronic calculation as described in Section 2.3 intractable. However, the properties of the potential-energy surfaces suggest that simplifications are possible. Equivalent minima are separated by relatively low barriers that permit the interconversions of neighboring structures by tunneling. In the following, the tunneling formalism is derived which is then used to predict the rovibronic energy levels including their symmetry.

The barrier height separating two enantiomeric C_{2v} structures has been calculated to be 5100 cm^{-1} at the UMP2/cc-pVDZ level of ab initio theory (4700 cm^{-1} including zero-point corrections). The barrier separating two C_{2v} minima in Figure 8 amounts to only 1010 cm^{-1} at the same level of theory and only 410 cm^{-1} after zero-point correction (although a harmonic zero-point correction is questionable

for a flat potential-energy surface). The motion connecting two enantiomeric structures corresponds to the stereomutation of the methane cation.[38,39] The resulting splittings are estimated to be less than 10^{-7} cm^{-1} and cannot be observed at our experimental resolution of 0.2 cm^{-1}. The motion connecting equivalent minima of a given set of six structures corresponds to a cyclic permutation of three hydrogen atoms also known as pseudorotation. The low barrier for this process implies that it must be observable at our resolution. Inspection of Figure 8 reveals that the feasible permutation–inversion operations are of the type E, (123), (12)(34), (12)*, (1234)* and form a group that is known as T_d(M).[22] The molecular symmetry group used in Ref. [40] contains operations of the type E, (123), (12)(34), (12), (1234), which is incorrect because the last two operations involve an odd number of permutations and thus interconvert enantiomers.

Tunneling between the six structures depicted in Figure 8 is conveniently described in a matrix representation using direct product basis states [Eq. (20)] where $|n\rangle$ is the adiabatic electronic state vector in the n^{th} potential well (given below each structure in Figure 8) and χ_n represents the vibrational ground-state function that is sharply localized in the vicinity of the n^{th} potential well.

$$\phi_n = |n\rangle|\chi_n\rangle \tag{20}$$

Neglecting the overlap between the vibrational basis functions and defining $\sigma = 1/2\langle\chi_1|\hat{H}_{\text{vib}}|\chi_2\rangle$ and $\langle\chi_1|\hat{H}_{\text{vib}}|\chi_1\rangle = 0$, where $\hat{H}_{\text{vib}}$ is the vibrational operator for the lowest potential-energy surface, the effective Hamiltonian matrix can be expressed as Equation (21)].

$$\mathbf{H}_{\text{vib}} = \begin{pmatrix} 0 & \sigma & -\sigma & \sigma & -\sigma & 0 \\ \sigma & 0 & \sigma & 0 & -\sigma & \sigma \\ -\sigma & \sigma & 0 & -\sigma & 0 & \sigma \\ \sigma & 0 & -\sigma & 0 & \sigma & \sigma \\ -\sigma & -\sigma & 0 & \sigma & 0 & \sigma \\ 0 & \sigma & \sigma & \sigma & \sigma & 0 \end{pmatrix} \tag{21}$$

The tunneling eigenstates of CH_4^+ are obtained by diagonalizing $\mathbf{H}_{\text{vib}}$ and form two sets of triply degenerate levels with eigenvalues E_{F_2} and E_{F_1} [Eq. (22)] separated by the tunneling splitting $\delta = 4|\sigma|$ (σ is negative).

$$\begin{aligned} E_{F_2} &= +2\sigma \\ E_{F_1} &= -2\sigma \end{aligned} \tag{22}$$

The subscript indicates the symmetry of the vibronic wavefunction in the T_d(M) group. The high permutational symmetry of CH_4^+ is responsible for the equality of all matrix elements $\langle\chi_i|\hat{H}_{\text{vib}}|\chi_i\rangle$ and all tunneling elements $\langle\chi_i|\hat{H}_{\text{vib}}|\chi_j\rangle$. Each component of the triply degenerate vibronic wavefunctions has amplitudes in four of the minima.[41]

The vibronic ground-state wavefunctions of both the cyclopentadienyl cation and the methane cation are delocalized over areas of the potential-energy surfaces that correspond to different but equivalent molecular structures. Group theoretical methods can be used to predict the symmetries of the vibronic wavefunctions. First, the barriers separating equivalent minima are assumed to be infinitely high and the symmetry of the vibronic wavefunction is determined locally. Since the molecule is rigid and in its ground vibrational state, it must be classified in the point group of the distorted structure and the vibronic symmetry is the same as its electronic symmetry. This is B_2 in the case of CH_4^+, as can be seen from the structure of the singly occupied molecular orbital displayed in Figure 6. In defining the symmetry, we have used the C_{2v} character table given in Ref. [42]. If tunneling is taken into account, the vibronic symmetries must be classified in the CNPI or the MS group and are obtained by correlating the irreducible representations of C_{2v} to T_d(M). B_2 becomes $F_2 \oplus F_1$ which is in agreement with the result of the tunneling matrix in Equation (21). This procedure can also be used to derive the vibronic symmetries of the partially deuterated methane cations, as will be explained in Section 5.1.

3. Experimental Methods

The investigation of molecular ions by direct spectroscopy is a challenging task. Indeed, the repulsion forces between cations in a gas sample limit their concentration to below 10^{10} cm^{-3}, and cause undesired Doppler broadenings of the transitions. Moreover, the techniques used to generate the cations (electron impact ionization, discharges, etc.) are neither chemically nor state selective and the extraction of relevant spectral features from experimental data represents a real challenge. In photoelectron spectroscopy, the cation energy-level structure is measured from the neutral ground state of the molecule. Efficient and chemically selective routes exist to produce neutral species and supersonic expansions can lead to the population of only the lowest quantum states. Moreover, the photoionizing transitions to specific cationic states can be detected with almost 100% efficiency by measuring the electrons.

In PFI-ZEKE photoelectron spectroscopy, electrons produced by the electric field ionization of very high Rydberg states (principal quantum number $n \approx 300$) are measured as a function of the wavenumber of a tunable light source.[20,21,43,44] The lines in a PFI-ZEKE photoelectron spectrum are located just below each ionization threshold and thus directly map out the relative positions of the ionic energy levels. To obtain the field-free ionization thresholds, a correction has to be applied.[45]

The experimental setup has been described in Ref. [37]. Briefly, the neutral molecules in a supersonic expansion are photoexcited inside a stack of resistively coupled extraction plates. For photoionization measurements, the produced ions are extracted using a pulsed voltage toward a multichannel plate detector where they are detected mass-selectively. For PFI-ZEKE experiments, an electric field pulse sequence consisting typically of a discrimination pulse of $+0.05$ V cm^{-1} and a detection pulse of -0.2 V cm^{-1} delayed by 3 μs with respect to photoexcitation was used, resulting in a resolution of 0.3 cm^{-1}.

To simplify the PFI-ZEKE photoelectron spectra and to provide an experimental assignment of the rovibronic symmetry of the observed cationic levels, various double-resonance excitation schemes were used. The resonance-enhanced two-photon excitation/ionization experiments were carried out using two tunable laser sources. The laser beams crossed the molecular beam at right angles in a counter-propagating arrangement. By scanning the first laser at a constant wavenumber of the second laser, spectra of the intermediate state were recorded. PFI-ZEKE photoelectron spectra were measured from selected vibrational levels of the intermediate level by fixing the wavenumber of the first laser at the appropriate spectral position and scanning the wavenumber of the second laser.

Two schemes were used to assign the nuclear spin species and the rovibronic symmetry of the ionic levels experimentally. The first technique, that we call "ZEKE-dip" spectroscopy (by analogy with ion-dip spectroscopy[46]) was applied to assign the rovibronic symmetries of the levels of the methane cation. It consists in holding the vacuum-UV (VUV) frequency at the position of a given line in the single-photon PFI-ZEKE photoelectron spectrum, and monitoring the depletion of the photoelectron signal at specific frequencies of an IR laser that is resonant with rovibrational transitions in the ν_3 or $2\nu_3$ bands of neutral methane. A depletion of up to 50% of the original signal indicated that the IR and the VUV photoelectronic transitions had a common rovibrational lower level that is easily identifiable by comparison with the well-known IR spectrum of CH_4.[47] In the second technique, the IR frequency was held at the position of specific lines of the IR spectrum, and the VUV frequency was scanned across the ionization thresholds. With these two methods, nuclear spin symmetries could be assigned to most lines in the PFI-ZEKE photoelectron spectrum (the nuclear spin symmetry is assumed to be conserved during photoionization).

The investigation of the cyclopentadienyl cation required the production of the cyclopentadienyl radical under conditions that are compatible with PFI-ZEKE photoelectron spectroscopy. Such a source has been developed recently.[48] The cyclopentadienyl radicals were produced by photolysis of cyclopentadiene with the 248 nm output of a KrF excimer laser (Lambda Physik, CompEx) in a quartz capillary mounted at the end of a pulsed nozzle.[34,48,49] The cyclopentadienyl radicals were cooled in the pulsed supersonic expansion into vacuum to rotational temperatures around 8 K. The supersonic beam was skimmed and then intersected by the VUV laser beam at right angles in the photoionization region. Cyclopentadiene was produced from dicyclopentadiene (Fluka) through distillation and stored at −78 °C until used. It was introduced in a stream of neat helium into the nozzle reservoir at a stagnation pressure of 5 bar.

4. Comparison with Experimental Data

The theoretical considerations presented in Section 2 explained how the JT and PJT effects lower the potential energy for nuclear arrangements of reduced symmetry. In CH_4^+ and $C_5H_5^+$ and their deuterated isotopologues, different equivalent minima appear with small to vanishing barriers between them. Consequently, a molecule subject to a JT effect often samples several equivalent distorted geometries which results in complex spectra. This section illustrates the spectroscopic signatures of this fluxionality caused by the JT effect. The spectroscopic experiments serve the purpose of determining the quantum-level structure of the molecular cation including nuclear spin symmetry which provides information on the structure and the dynamics of the molecule.

4.1. Cyclopentadienyl Cation

Prior to our investigations by PFI-ZEKE photoelectron spectroscopy[34,49] the cyclopentadienyl cation had only been studied in the condensed phase by electron paramagnetic resonance spectroscopy.[50] The excitation schemes used in our experiments are represented in Figure 9. Direct one-photon

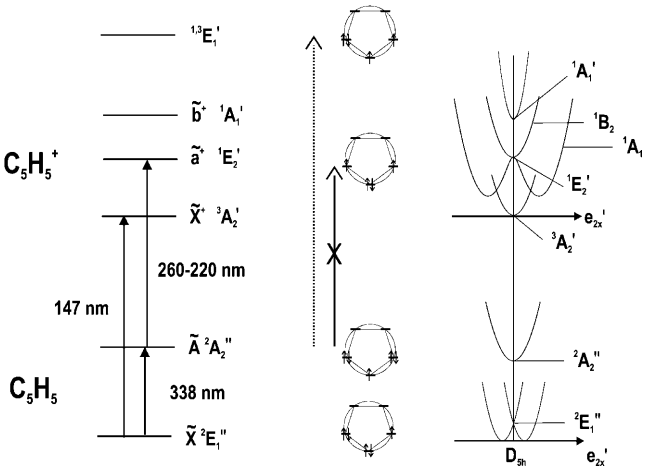

Figure 9. One- and two-photon excitation schemes used to record photoionization and PFI-ZEKE photoelectron spectra of the cyclopentadienyl radical. The positions of the low-lying electronic states of the cyclopentadienyl radical and cation are represented on the left-hand side by the horizontal lines next to the corresponding spectroscopic and symmetry labels. The main electronic configurations of the π molecular orbitals from which the electronic states derive are represented schematically in the central column. The right-hand side represents schematic cuts through the potential energy surface of the electronic states along nuclear displacements of e_2' symmetry (adapted from Ref. [34]).

excitation in the VUV from the $\tilde{X}\,^2E_1''$ ground state of the cyclopentadienyl radical enabled us to record the PFI-ZEKE photoelectron spectrum of the ground state of the cyclopentadienyl cation.[49] The spectrum is dominated by the transition to the vibrational ground state of the cation. Since the Jahn–Teller distortion of the electronic $^2E_1''$ ground state of the radical is relatively weak, this observation indicates that the $\tilde{X}^{+3}A_2'$ ground state of the cyclopentadienyl cation is insignificantly distorted away from the D_{5h} structure. A second excitation scheme was used to characterize higher lying electronic states. (1 + 1′)-two-photon resonant excitation through different vibrational levels of the electronically

excited $\tilde{A}\,^2A_2''$ state of the neutral radical gave access to a dense progression of vibrational levels beginning about 1500 cm^{-1} above the measured origin of the $^3A_2'$ state.[49] Figures 10a and b show the PFI-ZEKE photoelectron spectra recorded following excitation through the vibrational ground

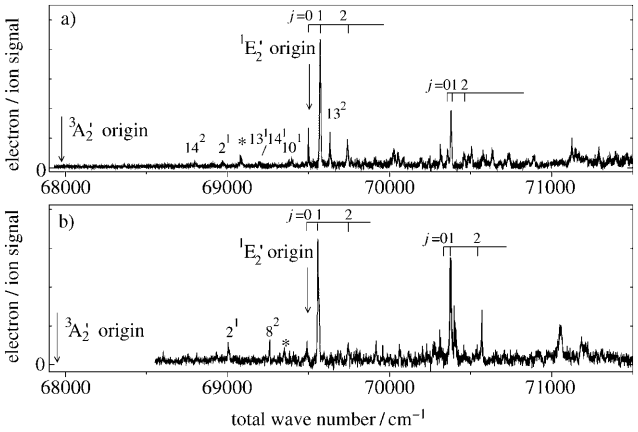

Figure 10. Two-photon resonant PFI-ZEKE photoelectron spectra recorded through the vibrationless level of the $\tilde{A}\,^2A_2''$ state of a) C_5H_5 and b) C_5D_5. Vertical arrows mark the positions of the adiabatic ionization thresholds corresponding to the formation of the $\tilde{X}^+\,^3A_2'$ and lower component of the $\tilde{a}^+\,^1E_2'$ states. The horizontal axis corresponds to the sum of the wavenumbers of both lasers. Excited vibrational levels of the $\tilde{X}^+\,^3A_2'$ state are assigned in harmonic notation whereas the pseudorotational levels of the lower component of the $\tilde{a}^+\,^1E_2'$ state are assigned in terms of the vibronic angular-momentum quantum number j (adapted from Ref. [34]).

state of the $^2A_2''$ state of the neutral radicals C_5H_5 and C_5D_5, respectively. The vertical arrows on the low wavenumber side of Figure 10 correspond to the positions where the origin of the $^3A_2'$ has been observed in the single-photon PFI-ZEKE experiments.[49] The origins of the $\tilde{X}^+ \leftarrow \tilde{X}$ photoelectron band systems are not observed in the two-photon experiments but several vibrationally excited levels of the $\tilde{X}^+\,^3A_2'$ electronic state are observed: 14^2, 2^1, 13^1, 14^1, 10^1, and 13^2 in $C_5H_5^+$ and 2^1, 8^2 in $C_5D_5^+$. At a total wavenumber of approximately 69500 cm^{-1}, the origin of the $\tilde{a}^+\,^1E_2' \leftarrow \tilde{X}$ photoelectron band system is observed in both molecules as a rather weak line (labeled "$j=0$") immediately followed by a much more intense line (labeled $j=1$) and further weak lines. A second similar group of lines is observed at higher wavenumbers around 70400 cm^{-1}. The lines of these two progressions are assigned in terms of the quantum number j which stands for the vibronic angular momentum.[34] The upper progression is attributed to the excited vibrational level with one quantum of excitation along the radical dimension of the potential trough displayed in Figure 3. The separation between the two lowest lines in the progressions amounts to only 71 cm^{-1} in $C_5H_5^+$ and 70 cm^{-1} in $C_5D_5^+$ which is characteristic of a very strong PJT distortion and the associated free pseudorotation of the nuclear framework (see Figure 5). The motion along the trough in the lowest potential surface of Figure 3 is indeed expected to be unhindered as explained in Section 2.3. From the experimental observations it can be concluded that the quantized states corresponding to this motion have an energy proportional to j^2 with integer values of the vibronic-angular-momentum quantum numbers ($j=0,1,2\ldots$). In the case of a strong JT (as opposed to a PJT) distortion, the energy would also be proportional to j^2 but with half-integer values of j (1/2, 3/2…; see also Refs. [9–11]). The assignment of the spectra displayed in Figure 10 relied on ab initio quantum chemical calculations, vibronic coupling calculations, and rotationally resolved measurements.[34]

The unexpected intensity distribution originates from the fact that the photoionizing transition from the $^2A_2''$ state to the $^1E_2'$ state of the cation is forbidden, as it is formally a two-electron transition (see Figure 9). The allowed photoionizing transitions from the $^2A_2''$ state lead to the formation of ions in the $^1E_1'$ and $^3E_1'$ states with the configuration $((a_2'')^1(e_1'')^3(e_2'')^0)$. According to Equation (7) the $^1E_1'$ state of this configuration and the $^1E_2'$ state are vibronically coupled by modes of symmetry $e_1' \otimes e_2' = e_1' + e_2'$. Consequently, the e_2' modes that mediate the strong PJT effect also induce a Herzberg–Teller intensity borrowing that enables the observation of the transitions to the $^1E_2'$ state. This mechanism primarily lends intensity to the vibronic levels of symmetry e_1' or e_2' with $j>0$ but not to the $j=0$ level which is of a_1' vibronic symmetry.[34]

Our investigations of the cyclopentadienyl cation by high-resolution photoelectron spectroscopy provide the following picture of the structure and dynamics of this prototypical molecule. The ground state is of $^3A_2'$ symmetry and has a minimum-energy geometry belonging to the D_{5h} point group. This result contrasts with the naive expectation that an antiaromatic molecule should have C–C bonds of unequal lengths in its ground electronic state. The first excited electronic state is of symmetry $^1E_2'$. It is subject to a strong PJT interaction with the next-higher singlet state of symmetry $^1A_1'$ which stabilizes its lower component by approximately 4000 cm^{-1}. The potential-energy surface of the lower component of the $^1E_2'$ state is thus characterized by a deep trough (as shown schematically in Figure 3) that gives rise to free pseudorotation. In the cyclopentadienyl cation, the PJT effect thus causes a high fluxionality of the molecule by allowing a complete delocalization of the nuclear wavefunction.

This insight allows us to precisely describe the implications of antiaromaticity on a molecule. The triplet electronic state resulting from the lowest lying (e^2) electronic configuration does not distort because it is nondegenerate and no other triplet state results from this configuration. Thus all the C–C bond lengths are equal. The three singlet states (one $^1A_1'$ state and the two components of the E_2' state) may distort to geometries with unequal C–C bond lengths, but only through PJT interactions (see Figure 5). The corresponding stabilization may lower one singlet state below the triplet state, as is the case in cyclobutadiene.[51,52] In the cyclopentadienyl cation, the stabilization energy is not large enough to lower the singlet state below the triplet state which results in an undistorted triplet ground state. The chemical intuition of unequal bond lengths for an antiaromatic electronic configuration is thus only applicable to the lowest singlet state of these molecules. In this state, $C_5H_5^+$ distorts to form a dienylic and an allylic structure (see Figure 5b) which results in a localization of the electronic wavefunction and a delocalization of the nuclear wavefunction. The PJT effect can thus be

interpreted as the way the molecule takes to avoid the unfavorable antiaromatic electronic structure.

4.2. Methane Cation

The single-photon PFI-ZEKE photoelectron spectrum of methane is shown in Figure 11 (top trace). In spite of its simple appearance the rotational structure of this spectrum has long remained unassigned after its first observation in 1999.[53] An experimental assignment of the nuclear spin symmetries using infrared-VUV double-resonance methods has eventually permitted the assignment of the spectrum and enabled the characterization of the dynamics induced by the JT effect.[29,41] The experimental technique was described in Section 3 and consisted of two complementary methods. The first relied on fixing the VUV laser wavenumber at the position of a selected line of the PFI-ZEKE photoelectron spectrum and using an IR laser to saturate a rovibrational transition in the ground electronic state of the neutral molecule. A decrease of the PFI-ZEKE photoelectron signal indicated that the two transitions shared a common initial state, namely the lower state of the IR transition. This method allowed the identification of the rotational level of the vibronic ground state of methane (presented as symmetry labels above the lines of the top spectrum in Figure 11) from which the PFI-ZEKE transition originated. The second method consisted of exciting a specific rotational level of a vibrationally excited level of the neutral molecule and recording the PFI-ZEKE photoelectron spectrum from that selected level.

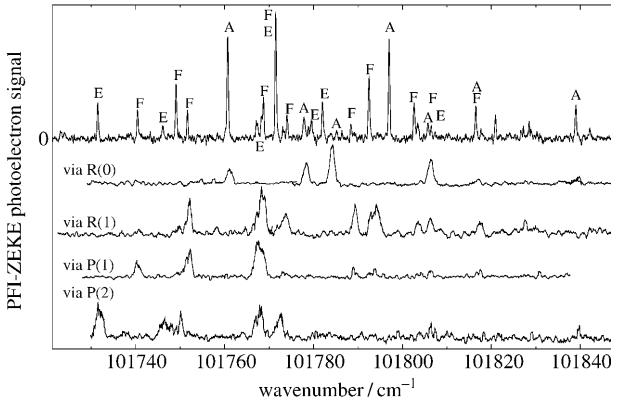

Figure 11. Top trace: Single-photon PFI-ZEKE photoelectron spectrum of CH_4 in the region of the adiabatic ionization threshold obtained using electric field pulses of $+86$ mV cm^{-1} and -138 mV cm^{-1}. Lower traces: two-photon IR + VUV PFI-ZEKE PE spectra recorded through selected rotational levels of the ν_3 fundamental using electric field pulses of $+17$ mV cm^{-1} and -860 mV cm^{-1}. The selected rotational line of the vibrational transition to the intermediate level is indicated above the spectra. The letters A, E, and F correspond to the experimentally assigned nuclear spin symmetries (A_1, E, or F_2; adapted from Ref. [41]).

$^{12}CH_4$ and $^{12}CH_4^+$ have three nuclear spin isomers with the nuclear spin symmetries in T_d(M) of A_1 (meta, $I=2$), E (para, $I=0$), and F_2 (ortho, $I=1$).[54,55] Meta methane exists in levels of rovibronic symmetry A_1 or A_2, para methane in levels of symmetry E and ortho methane in levels of symmetry F_1 or F_2. Under the jet-cooled conditions of our experiments, only the three lowest rotational levels of the neutral vibronic ground state are populated, corresponding to the rotational quantum numbers and nuclear spin symmetries $J=0$ (A_1), $J=1$ (F_2), and $J=2$ (E). Because electric dipole transitions only connect levels of the same nuclear spin symmetry, the identification of the initial state of the PFI-ZEKE photoelectron transition permits the assignment of the nuclear spin symmetry in the cation, that is, the rovibronic symmetry without the index (A_1 and A_2 are not distinguished, nor F_1 and F_2). In the case of a resonant two-photon excitation, the first transition can only populate levels of the same nuclear spin symmetry as the initial level and the same principle applies.

The spectra obtained after two-photon resonant excitation are displayed in the four lower traces of Figure 11. The knowledge of the initial state allows a map of the energy levels to be constructed on an absolute energy scale (sorted by nuclear spin symmetry) which can then be compared with calculations. The result is displayed in Figure 12 where the left-hand side (Figure 12a) represents the experimentally determined level positions with respect to the neutral rovibronic ground state, and the right-hand side (Figure 12b) the results of a calculation using an effective rotation-tunneling Hamiltonian.[29,41] There is a one-to-one correspondence between the calculated and experimental values of the levels of A and E symmetry up to $N^+=3$. The calculations predict more F levels than observed experimentally, but the grouping of calculated F levels reflects the experimental structure. It is likely that not all levels could be observed as a result of the resolution and sensitivity limits of the experiment. The adjustable parameters in the model Hamiltonian of Refs. [29,41] were 1) three rotational constants ($A=6.40(13)$, $B=5.55(9)$, $C=4.03(6)$ cm^{-1}) that essentially correspond to the rotational constants of the distorted C_{2v} structure of the potential minima, 2) the tunneling splitting ($\delta=4|\sigma|=$

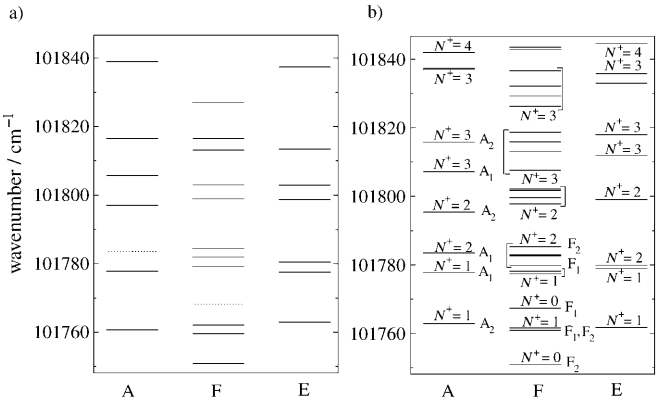

Figure 12. Comparison of the experimentally determined level structure of CH_4^+ (a) with the eigenvalues of a tunnel–rotation Hamiltonian (b; see Ref. [29]). The wavenumber scale is defined with respect to the ground state of CH_4 (adapted from Ref. [41]).

16.4(40) cm^{-1}) defined in Equation (22), and 3) the ionization energy $E_I/(hc) = 101\,752(15)\ cm^{-1}$. The comparison between the calculations and the experiment suggests that the effective rotation–tunneling Hamiltonian captures the essential aspects of the dynamics of the molecule and correctly incorporates the Jahn–Teller effect. The structure and dynamics of the ground state of CH_4^+ are characterized by a large-amplitude tunneling motion connecting equivalent minima of C_{2v} geometry. The $N^+ = 0$ ground state of CH_4^+ is a tunneling doublet of triply degenerate levels and the lowest level has nuclear spin symmetry F_2 (also F_2 rovibronic symmetry according to the theoretical considerations presented in Section 2.4).

The results of our investigations of the methane cation by high-resolution photoelectron spectroscopy can thus be summarized in terms of a dynamic structure. The JT effect causes a distortion of the molecule away from the tetrahedral symmetry towards a distorted structure of C_{2v} symmetry. Rather than a single minimum, there are two enantiomeric sets of six equivalent minima and the molecule may be described as having a highly fluxional structure resulting from the tunneling between the structures of each set on the picosecond time scale. The sequence of tunneling levels, F_2 below F_1, is characteristic of the JT effect in a threefold degenerate electronic state, and results from a geometric phase effect.[29] The level structure for tunneling between six equivalent minima on a nondegenerate electronic surface (as in the case of a PJT effect with an electronically nondegenerate lower state) would be A_1, F_2, E.

Without the JT effect, CH_4^+ would have a rigid tetrahedral structure and the electron hole in the valence shell would be delocalized over three equivalent molecular orbitals of symmetry f_2 (aligned along the three C_2 axes of the molecule). In the presence of the JT effect, the electron hole is localized in a single molecular orbital (see Figure 6) while the nuclear wavefunctions are delocalized over 12 equivalent potential-energy minima of C_{2v} symmetry. The methane cation shares several common properties with the cyclopentadienyl cation. The JT effect induces a high fluxionality of the molecular structure and causes simultaneously an electronic localization and a nuclear delocalization. In both cases, the JT (or PJT) distortions can be rationalized by chemical intuition: in the case of the $^1E_2'$ state of the cyclopentadienyl cation the distortion enables the molecule to avoid the unfavorable delocalized antiaromatic electronic structure by forming dienylic and allylic structures. In the case of CH_4^+, the distortion towards a CH_2^+-H_2 complex (see Figure 6) can be understood by consideration of the low ionization energy of CH_2.[56]

5. Isomerism and Chirality

5.1. Isomerism in CH_3D^+ and $CH_2D_2^+$

Partial isotopic substitution reduces the symmetry of the vibrational Hamiltonian without affecting the electronic degrees of freedom. It provides additional insights into vibronic coupling problems because the permutational symmetry is reduced and vibrational zero-point energy effects make otherwise equivalent minima distinguishable. Partial isotopic substitution of JT systems has been a very useful tool in determining the distorted equilibrium structure of molecules undergoing an E⊗e Jahn–Teller effect, such as the cyclooctatetraene anion,[57] the benzene anion,[58] benzene,[59] and the cyclopentadienyl radical.[60]

Partial deuteration of CH_4^+ removes the equivalence of the six minima represented in Figure 8 because of the different zero-point energies of the resulting structures. If the hydrogen atom labeled "4" in Figure 8 is replaced by a deuterium atom, the structures **1**, **2**, and **3** remain equivalent, as do minima **4**, **5**, and **6** but the two sets are distinguishable. In the treatment that led to Equation (21), the tunneling matrix elements presented in Equation (23) must be considered for CH_3D^+.

$$\begin{aligned}
&\langle\chi_i|\hat{H}|\chi_i\rangle &&= 0 \text{ for } i \in \{\mathbf{1},\mathbf{2},\mathbf{3}\}\\
&\langle\chi_i|\hat{H}|\chi_i\rangle &&= \Delta \text{ for } i \in \{\mathbf{4},\mathbf{5},\mathbf{6}\}\\
&1/2\langle\chi_i|\hat{H}|\chi_j\rangle &&= \sigma \text{ for } i\neq j,\ \{i,j\} \in \{\mathbf{1},\mathbf{2},\mathbf{3}\}\\
&1/2\langle\chi_i|\hat{H}|\chi_j\rangle &&= \sigma' \text{ for } i\neq j,\ \{i,j\} \in \{\mathbf{4},\mathbf{5},\mathbf{6}\}\\
&1/2\langle\chi_i|\hat{H}|\chi_j\rangle &&= \sigma'' \text{ for } i\neq j,\ i \in \{\mathbf{1},\mathbf{2},\mathbf{3}\},\ j \in \{\mathbf{4},\mathbf{5},\mathbf{6}\} \text{ or vice versa}
\end{aligned} \tag{23}$$

The subscripts i and j refer to the structures drawn in Figure 8, σ, σ', and σ'' are all negative, and Δ corresponds to the zero-point energy difference between the structures of both sets. The tunneling matrix for CH_3D^+ thus takes the form given in Equation (24)[*] and has the eigenvalues given by Equations (25).

$$\mathbf{H}_{\text{vib}} = \begin{pmatrix}
0 & \sigma & -\sigma & \sigma'' & -\sigma'' & 0\\
\sigma & 0 & \sigma & 0 & -\sigma'' & \sigma''\\
-\sigma & \sigma & 0 & -\sigma'' & 0 & \sigma''\\
\sigma'' & 0 & -\sigma'' & \Delta & \sigma' & \sigma'\\
-\sigma'' & -\sigma'' & 0 & \sigma' & \Delta & \sigma'\\
0 & \sigma'' & \sigma'' & \sigma' & \sigma' & \Delta
\end{pmatrix} \tag{24}$$

$$E_{\text{E}} = \frac{1}{2}(\sigma - \sigma' + \Delta - S) \tag{25a}$$

$$E_{\text{A}_2} = -2\sigma \tag{25b}$$

$$E_{\text{A}_1} = 2\sigma' + \Delta \tag{25c}$$

$$E_{\text{E}} = \frac{1}{2}(\sigma - \sigma' + \Delta + S) \tag{25d}$$

In Equations (25a)–(25d), the symmetry labels given as subscripts correspond to the irreducible representations of the corresponding eigenvectors in C_{3v}(M), and S is defined by Equation (26)[**].

$$S = \sqrt{(\sigma+\sigma')^2 + 12\sigma''^2 - 2(\sigma+\sigma')\Delta + \Delta^2} \tag{26}$$

[*] Equation (4) of Ref. [61] represents the tunneling matrix corresponding to Figure 1 of that article, but with structures **4** and **5** reversed.

[**] Note that Equations (6) and (7) in Ref. [61] have been mistyped.

In the limit $|\sigma|$, $|\sigma'|$, $|\sigma''| \ll \Delta$ Equation (27) is obtained and the eigenvalues converge to those presented in Equations (28).

$$S \approx \Delta - (\sigma + \sigma') + \frac{(\sigma + \sigma')^2 + 12\sigma''^2}{2\Delta} \approx \Delta - (\sigma + \sigma') \tag{27}$$

$$E_E = \sigma \tag{28a}$$

$$E_{A_2} = -2\sigma \tag{28b}$$

$$E_{A_1} = 2\sigma' + \Delta \tag{28c}$$

$$E_E = -\sigma' + \Delta \tag{28d}$$

These energy levels correspond to two tunneling pairs ((E,A_2) and (A_1,E), respectively) with tunneling splittings $\delta = 3|\sigma|$ and $\delta' = 3|\sigma'|$, respectively. The tunneling states are represented schematically in Figure 13. If $|\Delta|$ is large compared to the tunneling matrix elements as is the case in CH_3D^+, the interconversion of one of the equilibrium structures **1**, **2**, and **3** into one of the structures **4**, **5**, and **6** is suppressed and two isomers exist. Minima **1**, **2**, and **3** have a short C–D bond and are designated as $CH_3D_s^+$ whereas minima **4**, **5**,and **6** have a long C–D bond and are designated as $CH_3D_\ell^+$.

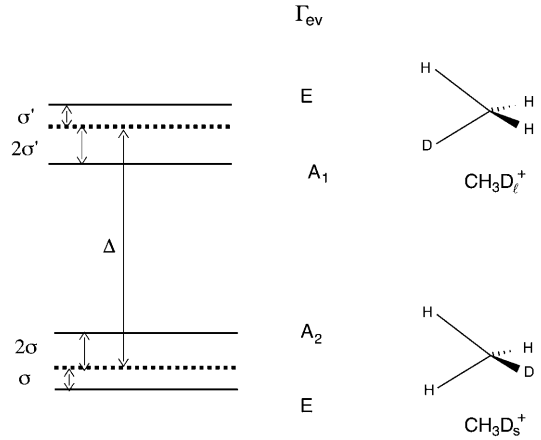

Figure 13. Tunneling levels of CH_3D^+ with zero total angular momentum (solid lines). The quantities σ und σ' represent the tunneling integrals for the isomers $CH_3D_s^+$ and $CH_3D_\ell^+$, respectively, ZPED stands for the zero-point energy difference between these isomers, and Δ describes the zero-point energy difference in the absence of tunneling (adapted from Ref. [61]).

The vibronic symmetries can also be predicted by group theory as outlined in Section 2. The ordering of the orbitals and the shape of the singly occupied molecular orbital of CH_4^+ is not significantly affected by deuteration. Classification of the electronic symmetry of this orbital in the C_s point group appropriate to CH_3D^+ at the minimum-energy geometry gives A″ for $CH_3D_s^+$ where the plane of symmetry contains the two short bonds and A′ for $CH_3D_\ell^+$ where the plane of symmetry contains the two long bonds. By correlating these symmetries to the molecular symmetry group corresponding to feasible permutations of the three protons (C_{3v}(M)) the tunneling splittings $A_2 \oplus E$ for $CH_3D_s^+$ and $A_1 \oplus E$ for $CH_3D_\ell^+$ are predicted in accordance with the tunneling calculations described above.

The PFI-ZEKE photoelectron spectrum of CH_3D is displayed in Figure 14. The bands labeled A and B have been assigned to the isomers $CH_3D_s^+$ and $CH_3D_\ell^+$, respectively, on the basis of their tunnel–rotational structures.[61]

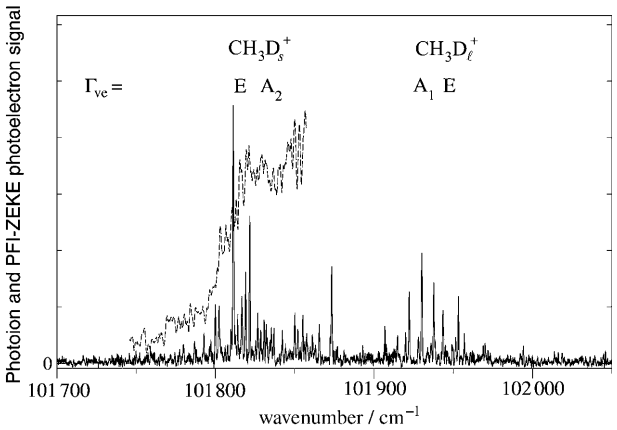

Figure 14. PFI-ZEKE photoelectron spectrum (solid line) and photoionization spectrum (dashed line) of CH_3D. The PFI-ZEKE photoelectron spectrum was recorded using a sequence of pulsed electric fields of $+35\ mVcm^{-1}$ and $-130\ mVcm^{-1}$. The two bands are assigned to the two isomers $CH_3D_\ell^+$ and $CH_3D_s^+$.

Band A consists of transitions to a tunneling doublet of vibronic levels E and A_2 whereas band B consists of transitions to a tunneling doublet A_1 and E. The experimentally determined zero-point energy difference amounts to $121(1)\ cm^{-1}$ which agrees with the value of $114\ cm^{-1}$ calculated at the CCSD(T)/cc-pVTZ level of ab initio theory. The tunneling splittings (equal to $|3\sigma^{(\prime)}|$) are much smaller and amount to 9.6 and $6.6\ cm^{-1}$, respectively, as determined from the experimental spectrum. In each of these isomers, the hydrogen atoms exchange on a picosecond time scale and are therefore equivalent on the time scale of our experiments. Hence, CH_3D^+ indeed appears to have two distinct isomers that must have different chemical properties.

The symmetry is lowered even further if two hydrogen atoms are replaced by deuterium atoms. In the treatment that led to Equation (21), the tunneling matrix elements in Equation (29) must therefore be considered for $CH_2D_2^+$.

$$\begin{aligned}
&\langle\chi_i|\hat{H}|\chi_i\rangle \quad = 0 \text{ for } i = \mathbf{1}\\
&\langle\chi_i|\hat{H}|\chi_i\rangle \quad = \Delta \text{ for } i \in \{\mathbf{2},\mathbf{3},\mathbf{4},\mathbf{5}\}\\
&\langle\chi_i|\hat{H}|\chi_i\rangle \quad = \Delta' \text{ for } i = \mathbf{6}\\
&1/2\langle\chi_i|\hat{H}|\chi_j\rangle = \sigma \text{ for } i \neq j,\ \{i,j\} \in \{\mathbf{2},\mathbf{3},\mathbf{4},\mathbf{5}\}\\
&1/2\langle\chi_i|\hat{H}|\chi_j\rangle = \sigma' \text{ for } i \neq j,\ i = \mathbf{1},\ j \in \{\mathbf{2},\mathbf{3},\mathbf{4},\mathbf{5}\} \text{ or vice versa}\\
&1/2\langle\chi_i|\hat{H}|\chi_j\rangle = \sigma'' \text{ for } i \neq j,\ i = \mathbf{6},\ j \in \{\mathbf{2},\mathbf{3},\mathbf{4},\mathbf{5}\} \text{ or vice versa,}
\end{aligned} \tag{29}$$

In Equation (29) the subscripts i and j refer to the structures in Figure 8, σ, σ' und σ'' are all negative, and Δ

and Δ' correspond to the zero-point energy difference between the structures **1** and **2–5** and between **1** and **6**, respectively. The tunneling matrix for $CH_2D_2^+$ thus takes the form given by Equation (30) and has the eigenvalues (and approximate values in the case $(|\sigma'|, |\sigma''|) \ll (\Delta, \Delta')$) given by Equations (31).

$$\mathbf{H}_{\text{tun}} = \begin{pmatrix} 0 & \sigma' & -\sigma' & \sigma' & -\sigma' & 0 \\ \sigma' & \Delta & \sigma & 0 & -\sigma & \sigma'' \\ -\sigma' & \sigma & \Delta & -\sigma & 0 & \sigma'' \\ \sigma' & 0 & -\sigma & \Delta & \sigma & \sigma'' \\ -\sigma' & -\sigma & 0 & \sigma & \Delta & \sigma'' \\ 0 & \sigma'' & \sigma'' & \sigma'' & \sigma'' & \Delta' \end{pmatrix} \tag{30}$$

$$E_{B_2} = \frac{1}{2}(\Delta - S_1) \approx -\frac{4\sigma'^2}{\Delta} \tag{31a}$$

$$E_{A_1} = 2\sigma + \Delta \tag{31b}$$

$$E_{B_1} = \frac{1}{2}(\Delta + \Delta' - S_2) \approx \Delta - \frac{4\sigma''^2}{\Delta' - \Delta} \tag{31c}$$

$$E_{B_2} = \frac{1}{2}(\Delta + S_1) \approx \Delta + \frac{4\sigma'^2}{\Delta} \tag{31d}$$

$$E_{A_2} = -2\sigma + \Delta \tag{31e}$$

$$E_{B_1} = \frac{1}{2}(\Delta + \Delta' + S_2) \approx \Delta' + \frac{4\sigma''^2}{\Delta' - \Delta} \tag{31f}$$

S_1 and S_2 are given by Equations (32).

$$\begin{aligned} S_1 &= \sqrt{(\Delta^2 + 16\sigma'^2)} \\ S_2 &= \sqrt{(\Delta^2 - 2\Delta\Delta' + \Delta'^2 + 16\sigma''^2)} \end{aligned} \tag{32}$$

In the limit $(|\sigma'|, |\sigma''|) \ll (\Delta, \Delta')$, the eigenvalues can be further approximated by Equations (33 a–f)

$$E_{B_2} = 0 \tag{33a}$$

$$E_{A_1} = 2\sigma + \Delta \tag{33b}$$

$$E_{B_1} = \Delta \tag{33c}$$

$$E_{B_2} = \Delta \tag{33d}$$

$$E_{A_2} = -2\sigma + \Delta \tag{33e}$$

$$E_{B_1} = \Delta' \tag{33f}$$

and the corresponding eigenvectors are given by Equation (34) where the columns represent the eigenvectors in the same order as the eigenvalues given in Equation (33). The first and the last eigenvalues correspond to eigenvectors that are localized in minima **1** and **6**, belonging to the isomers $CH_\ell H_\ell D_s D_s^+$ and $CH_s H_s D_\ell D_\ell^+$, respectively. The four intermediate eigenvalues correspond to the isomer $CH_\ell H_s D_\ell D_s^+$ as shown schematically in Figure 15.

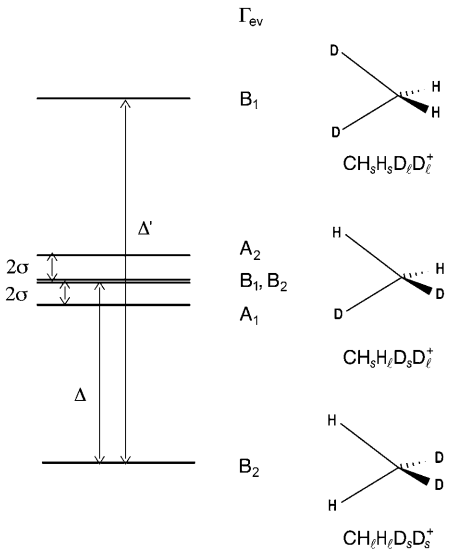

Figure 15. Tunneling levels of $CH_2D_2^+$ with zero total angular momentum (solid lines). The quantity σ represents the tunneling integral for the isomers $CH_\ell H_s D_\ell D_s^+$. Δ and Δ' describe the zero-point energy differences in the absence of tunneling.

$$\mathbf{U} = \frac{1}{2}\begin{pmatrix} 2 & 0 & 0 & 0 & 0 & 0 \\ 0 & -1 & 1 & -1 & 1 & 0 \\ 0 & -1 & 1 & 1 & -1 & 0 \\ 0 & 1 & 1 & -1 & -1 & 0 \\ 0 & 1 & 1 & 1 & 1 & 0 \\ 0 & 0 & 0 & 0 & 0 & 2 \end{pmatrix} \tag{34}$$

Figure 16 shows the PFI-ZEKE photoelectron spectrum of CH_2D_2 in the region of the adiabatic ionization threshold. Three bands labeled A, B, and C can be distinguished that have a very different (tunnel-)rotational structure. The separation between the centers of the bands A and B amounts to approximately 130 cm^{-1} and the separation between the bands A and C is 240 cm^{-1}. The calculated difference in zero-

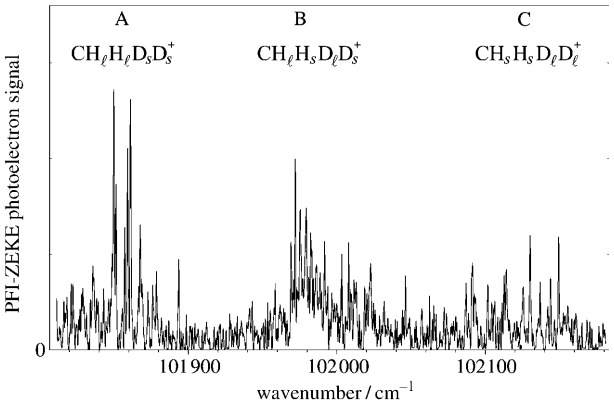

Figure 16. PFI-ZEKE photoelectron spectrum of CH_2D_2. The PFI-ZEKE photoelectron spectrum was recorded using a sequence of pulsed electric fields of $+35$ mVcm^{-1} and -160 mVcm^{-1}. The three bands are assigned to the three isomers $CH_\ell H_\ell D_s D_s^+$, $CH_\ell H_s D_\ell D_s^+$, and $CH_s H_s D_\ell D_\ell^+$.

point energies between the isomers $CH_\ell H_\ell D_s D_s^+$ and $CH_\ell H_s D_\ell D_s^+$ is 115 cm^{-1} and that between $CH_\ell H_\ell D_s D_s^+$ and $CH_s H_s D_\ell D_\ell^+$ is 220 cm^{-1} at the UMP2/cc-pVDZ level of ab initio theory. Consequently, the attribution of bands A, B, and C to the three isomers appears justified.

The isomers $CH_\ell H_\ell D_s D_s^+$ and $CH_s H_s D_\ell D_\ell^+$ have C_{2v} symmetry and their ground electronic states have $^2B_2$ and $^2B_1$ symmetry, respectively. Because these isomers are "rigid" on the time scale of our measurements,[62] their ground vibronic state must also have B_2 (B_1) symmetry, in agreement with results of the tunneling calculations. The structure of isomer $CH_\ell H_s D_\ell D_s^+$ has no symmetry elements and therefore belongs to the C_1 point group. Since the tunneling motion connecting the four equivalent minima (**2**, **3**, **4**, and **5** in Figure 8) is feasible, the molecular symmetry group of this isomer is C_{2v}(M). C_1 has a single irreducible representation that correlates with $A_1 \oplus A_2 \oplus B_1 \oplus B_2$ in C_{2v}(M) and the vibronic symmetries resulting from tunneling correspond to the four irreducible representations of C_{2v}(M) as obtained above.

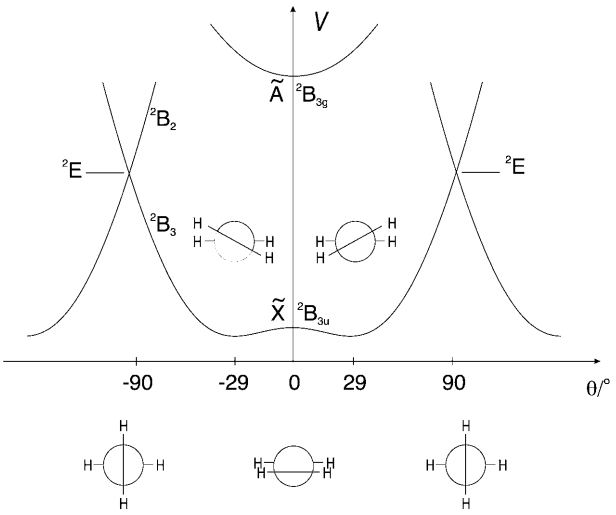

Figure 17. Schematic representation of the lowest potential-energy surfaces of the ethylene cation ($C_2H_4^+$). The vertical axis represents the electronic potential energy and the horizontal axis the angle θ between the two CH_2 planes.

5.2. The Jahn–Teller Effect and Chirality in $C_2H_4^+$ and $CH_2D_2^+$

The parity-violating nature of the electro-weak interaction is responsible for a small energy difference between two enantiomeric structures.[38,39,63,64] The influence of this effect on the dynamics of a chiral molecule depends on the relative magnitude of the parity-violating effect and the size of the tunneling splitting associated with stereomutation.

In many chiral molecules, such as methane derivatives with four different substituents or heavier analogues of hydrogen peroxide, tunneling splittings can be very small and two cases must be distinguished:[39,63] 1) If the parity-violating energy difference between the two enantiomers is much smaller than the splitting resulting from tunneling, then this splitting dominates the dynamics of the molecule in its ground state. The vibronic ground state of the molecule is delocalized over both minima of the potential energy surface. 2) If the tunneling splitting is much smaller than the parity-violating energy difference, the parity violation causes a localization of the vibronic ground state wavefunction in the potential-energy well corresponding to the more stable enantiomer. The next higher vibronic state is localized in the minimum corresponding to the other enantiomer. In this case the parity-violating interaction effectively breaks the symmetry of the molecule. The energy difference between the two enantiomeric structures induced by the electro-weak interactions effectively suppresses tunneling just like the difference in zero-point energies suppresses tunneling between minima corresponding to different isomers in CH_3D^+.

Distortions of the molecular geometry by the JT effect can induce chirality and in this section we discuss the cases of $C_2H_4^+$ and $CH_2D_2^+$. The ethylene cation has a nonplanar equilibrium structure.[65,66] The lowest potential-energy surfaces are represented schematically in Figure 17. Using the planar D_{2h} geometry as reference, the nonplanarity is a result of the vibronic coupling between the $\tilde{X}\ ^2B_{3u}$ and $\tilde{A}\ ^2B_{3g}$ mediated by the torsional mode of irreducible representation A_u. Alternatively, the distortion can also be considered to result from a JT effect that splits the ground $\tilde{X}\ ^2E$ state of D_{2d} geometry into two components of symmetry $^2B_3$ and $^2B_2$ in D_2 geometry. The $^2B_3$ component becomes the $\tilde{X}\ ^2B_{3u}$ state at the planar geometry, whereas the $^2B_2$ component becomes the $\tilde{C}\ ^2B_{2u}$ state (not shown).

Assuming that the barriers at both the D_{2h} and the D_{2d} geometry are impenetrable, the appropriate symmetry group for $C_2H_4^+$ is D_2. The electronic ground state is of $^2B_3$ geometry. Assuming that tunneling through the barrier at planarity (D_{2h} geometry) is feasible then the appropriate molecular symmetry group changes to D_{2h}(M), and the ground vibronic state splits into the tunneling doublet $B_{3u} \oplus B_{3g}$ which has indeed been observed experimentally.[66] If, on the contrary, tunneling were only possible through the barrier at D_{2d} geometry, the appropriate molecular symmetry group would be D_{2d}(M), and the vibronic ground state would have E symmetry. Therefore, even if the barrier at D_{2d} geometry were very low, there would not be any signature of tunneling. This situation is encountered in the allene cation.[67]

Since tunneling through the barrier at the D_{2d} geometry can be ignored, the dynamics of $C_2H_4^+$ can be qualitatively described by the two-minimum potential shown in Figure 17. The minimum energy structure has D_2 geometry and is chiral in the same way as H_2O_2, H_2S_2, Cl_2S_2, are chiral.[68–70] The structures corresponding to two adjacent minima are enantiomers of each other. The lowering of symmetry resulting from vibronic coupling thus induces chirality in a system that would otherwise be achiral. In the ethylene cation, the splitting associated with the tunneling motion through the D_{2h} barrier amounts to 83.7(5) cm^{-1} which corresponds to a stereomutation time of 200 fs. This motion clearly dominates the dynamics of the ground state of $C_2H_4^+$ and the separation of enantiomers is not possible. $C_2H_4^+$ clearly belongs to the first category of chiral molecules mentioned above. Indeed, the energy difference between the two enantiomeric struc-

tures of $C_2H_4^+$ caused by the electro-weak interaction is expected to be on the order of 10^{-13} cm^{-1} (which is the order of magnitude that was calculated for allene[71]). Substitution of the H atoms in $C_2H_4^+$ by heavier atoms may, however, provide further examples of molecules in the second category mentioned above.

The substituted methane derivatives represent an important class of chiral molecules.[38] Methane itself is not chiral in its ground vibronic state but its stereomutation, that is, the process that converts a structure with four numbered hydrogen atoms into its enantiomer, is important in understanding the dynamics of this class of chiral molecules. In the ground state of CH_4, the tunneling splitting resulting from this motion is expected to be very small because of the very high barrier ($\geq 35\,000$ cm^{-1}) for stereomutation.[72] In CH_4^+, the barrier for stereomutation is much lower.[35] We have calculated the lowest potential-energy surface of CH_4^+ at the UMP2/cc-pVDZ level of ab initio theory along the reaction path connecting a C_{2v} minimum energy structure to its enantiomeric structure using the algorithm implemented in Gaussian03.[73] The maximum of the reaction path corresponds to a structure of C_s geometry that is very similar to the one described in Ref. [35]. The purely electronic-barrier height is found to be 5100 cm^{-1} (4700 cm^{-1} after harmonic zero-point correction). The estimation of the tunneling splitting associated with stereomutation was performed using a WKB method[74] and the calculated reaction path and gave the value 10^{-7} cm^{-1} for this splitting.

What are the spectroscopic manifestations of stereomutation tunneling in CH_4^+? To obtain the appropriate molecular symmetry group, T_d(M) has to be extended to include operations that interconvert enantiomeric structures. The appropriate group contains all permutation-inversion operations of four particles and is designated S_4*[38] (Ref. [75] uses a different notation). The correlation of irreducible representations including spin-statistical weights for CH_4^+ and CD_4^+ are given in Tables 3 and 4, respectively. The Tables show that in CH_4^+, only the levels of rovibronic symmetry E will be split by stereomutation tunneling, whereas in CD_4^+, the E, the F_1, and the F_2 levels will be split. The statistical weights of (+) and (−) parity sublevels is equal in the E levels but different in the F_1 and F_2 levels.

The classification of chirality discussed so far is sufficient to describe the ground-state dynamics of chiral molecules characterized by tunneling between two minima corresponding to enantiomeric structures. The isomer $CH_\ell H_s D_\ell D_s^+$ of $CH_2D_2^+$ represents a special case of chirality, where eight potential-energy minima are isoenergetic if electro-weak interactions are ignored.

As explained in Section 4 in the discussion of CH_4^+, it can be expected that the potential-energy barriers separating the four structures shown in Figure 18 are much lower than the barrier for stereomutation. Consequently, the discussion will

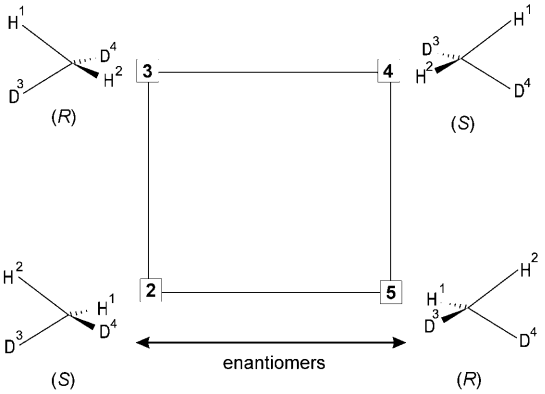

Figure 18. Topological representation of four equivalent minima of the isomer $CH_\ell H_s D_\ell D_s^+$ of $CH_2D_2^+$. The vertices correspond to the C_1 minimum-energy geometries and the edges to the equivalent pseudorotation–tunneling paths connecting the minima. Neighboring structures are enantiomers (disregarding the numbering) but diametrically opposed structures are identical. The chirality nomenclature used for axially chiral systems has been applied to label the structures.

Table 3: Correlation table of the rovibronic symmetries from the T_d(M) to the S_4* molecular symmetry group including nuclear spin statistical weights for $^{12}CH_4^+$.

T_d(M)	S_4*
A_1(5)	A_1^+(0)⊕A_2^-(5)
A_2(5)	A_2^+(5)⊕A_1^-(0)
E(2)	E^+(1)⊕E^-(1)
F_1(3)	F_1^+(3)⊕F_2^-(0)
F_2(3)	F_2^+(0)⊕F_1^-(3)

Table 4: Correlation table of the rovibronic symmetries from the T_d(M) to the S_4* molecular symmetry group including nuclear spin statistical weights for $^{12}CD_4^+$.

T_d(M)	S_4*
A_1 (15)	A_1^+(15)⊕A_2^-(0)
A_2 (15)	A_2^+(0)⊕A_1^-(15)
E(12)	E^+(6)⊕E^-(6)
F_1 (18)	F_1^+(3)⊕F_2^-(15)
F_2 (18)	F_2^+(15)⊕F_1^-(3)

be restricted to these four minima. As discussed in Section 5.1, tunneling between these four minima leads to a splitting of the four-fold degenerate ground vibronic state into a 1 + 2 + 1 pattern where the vibronic symmetries are A_1, B_1, B_2, and A_2. An inspection of the structures in Figure 18 reveals that directly adjacent structures are enantiomers of each other. Structures at opposite vertices of the diagram are identical except for the numbering of their substituents. The enantiomers can be labeled according to the nomenclature of axially chiral compounds (e.g., the asymmetrically substituted allene derivatives) because the substituent positions are pairwise equivalent in $CH_2D_2^+$. The structure corresponding to minimum **2** would thus be labeled (*S*)-$CH_\ell H_s D_\ell D_s^+$ whereas minimum **5** corresponds to (*R*)-$CH_\ell H_s D_\ell D_s^+$. Clearly, the fast pseudorotational tunneling connecting neighboring minima interconverts enantiomeric structures. In the following, we shall investigate how the tunneling dynamics affects the chirality of $CH_\ell H_s D_\ell D_s^+$ that is induced by the JT effect.

A closer inspection of the vibronic eigenfunctions associated with the B_1 and B_2 levels [see Eq. (34)] shows that they

correspond to symmetric and antisymmetric combinations of structures **2**, **4** and **3**, **5**, respectively. Indeed, the symmetric linear combination of the B_1 and B_2 functions is $\frac{1}{\sqrt{2}}(0,1,0,1)$ and the antisymmetric combination is $\frac{1}{\sqrt{2}}(1,0,1,0)$ (where the numbers in parentheses are the coefficients of the wavefunction in the basis $\{\phi_2,\phi_3,\phi_4,\phi_5\}$ of localized vibronic functions analogous to that defined in Equation (20) for CH_4^+). The first wavefunction corresponds to a pure *R*-enantiomer and the second to a pure *S*-enantiomer. A coherent superposition with the appropriate relative phase of the B_2 and B_1 vibronic levels would thus correspond to a single enantiomer.

We first consider the case where tunneling between inequivalent minima is negligible [$\sigma' = \sigma'' = 0$ in Eq. (30)]. In this case, the B_1 and B_2 levels are exactly degenerate and, consequently, the associated wavefunction can be chosen arbitrarily. Each enantiomer of $CH_\ell H_s D_\ell D_s^+$ would have a very long stereomutation time and could be isolated. However, the tunneling between inequivalent minima removes this accidental degeneracy and results in a splitting $E(B_2)-E(B_1) \approx 4(\sigma'^2/\Delta + \sigma''^2/(\Delta'-\Delta))$. The tunneling elements are expected to be on the order of 1 cm^{-1} whereas the zero-point energy differences are close to 100 cm^{-1}. The splitting of the nearly degenerate B_2 and B_1 levels will therefore be on the order of 0.1 cm^{-1}. An investigation, at high resolution, of the tunneling–rotational structure of band B in the spectrum shown in Figure 16 corresponding to the $CH_\ell H_s D_\ell D_s^+$ isomer would thus reveal interesting details about the unusual dynamics of chirality in this molecule.

6. A Related Fluxional System without Jahn–Teller Effects: CH_5^+

The group theoretical methods used above to predict the vibronic symmetries of tunneling levels in vibronically coupled systems have a broader range of applicability. They can also be applied to rovibronic states, are useful in the construction of correlation diagrams,[41,61] and may be used to treat non-Jahn–Teller fluxional systems. An important molecule that is closely related to the methane cation is protonated methane (CH_5^+), which is similar to CH_4^+ in that its hydrogen atoms exchange on a (sub)picosecond timescale. However, its ground electronic state has a closed-shell electronic structure, and CH_5^+ is therefore not subject to a JT effect. CH_5^+ has been of considerable interest to chemists because it is the prototype of hypercoordinated carbocations[76] and plays an important role in the chemistry of the interstellar medium.[77] Its infrared spectrum has been observed in laboratory experiments[78–80] but has not been conclusively assigned to date, though progress has been made recently towards establishing its vibrational energy-level structure theoretically.[81]

The lowest potential-energy surface of CH_5^+ is very flat and has several stationary points that lie close in energy (see, e.g., Refs. [82–87]) and are represented schematically in Figure 19. Recent calculations agree on a global minimum-energy structure of C_s symmetry and first-order saddle points of symmetries C_s and C_{2v} (the three structures are labeled

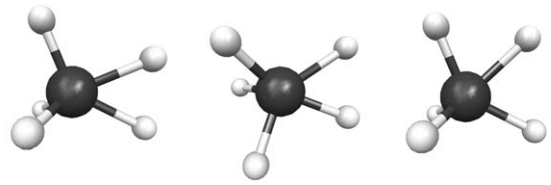

Figure 19. Stationary points of the lowest potential-energy surface of CH_5^+. Structure C_s(I) corresponds to a global-electronic-potential minimum whereas structures C_s(II) and C_{2v} correspond to low-lying saddle-points. The electronic potential-energy differences indicated are taken from Ref. [86].

C_s(I), C_s(II), and C_{2v} in Figure 19 and their relative electronic potential energies are indicated) but the ordering may change depending on the magnitude of the applied zero-point energy correction. A tunneling description is thus probably not fully adequate for the ground electronic state of CH_5^+. However, the strategy outlined in this Review, especially the group theoretical symmetry correlations, the determination of nuclear spin symmetries, and partial isotopic substitution are expected to provide additional help in the assignment of the complex spectra of CH_5^+ and its partially deuterated isotopologues.

We first assume that structure C_s(I) represented in Figure 19 is the global minimum-energy structure after zero-point correction. This structure belongs to the C_s point group and since the molecule has a closed-shell electronic structure, the irreducible representation of its rovibronic symmetry can only be A′. The CNPI group of CH_5^+ is $G_{240} = S_5 \otimes \{E, E^*\}$. By correlating the appropriate C_s point group to G_{240}, it is found that tunneling between all equivalent minima splits the ground state into ten sublevels with non-zero nuclear spin statistical weights (in parentheses) and degeneracies 1, 4, and 5, respectively: $A_2^-(6) \oplus G_2^+(4) \oplus 3\,G_2^-(4) \oplus 2\,H_2^+(2) \oplus 3\,H_2^-(2)$. The lowest-lying rotationally excited level (1_{01} in asymmetric top notation, rovibronic symmetry A″ in the C_s point group) splits into $A_2^+(6) \oplus 3\,G_2^+(4) \oplus G_2^-(4) \oplus 3\,H_2^+(2) \oplus 2\,H_2^-(2)$ (see also Ref. [88]). If, however, the structure of C_{2v} symmetry is the global minimum, the splitting of the ground state resulting from tunneling between the equivalent minima will be different. In the C_{2v} point group, the symmetry of the rovibronic ground state must be A_1 and the correlation to G_{240} gives $A_2^-(6) \oplus 2\,G_2^-(4) \oplus H_2^+(2) \oplus 2\,H_2^-(2)$, which is qualitatively different from the splitting obtained in the case of a minimum of C_s symmetry. The determination of nuclear spin symmetries as we have carried out for CH_4^+ and the identification of the rovibronic symmetries resulting from tunneling would therefore simplify the assignment of the high-resolution infrared spectra.[78,80]

As shown above, partial isotopic substitution suppresses tunneling between inequivalent minima in the methane cation which leads to the existence of isomers: two in the case of CH_3D^+ and CD_3H^+ and three in the case of $CH_2D_2^+$. In the case of CH_5^+, assuming the C_s structure (I) to be the minimum-energy geometry (see Figure 19), it is possible to

predict the number of isomers. This structure has only two equivalent hydrogen atoms, which are below and above the plane in Figure 19. CH_4D^+ and CHD_4^+ could thus have four isomers. If the only H (or D) atom occupies one of the two equivalent positions, a chiral structure results. $CH_3D_2^+$ and $CH_2D_3^+$ could have seven isomers. If the two equivalent positions are occupied by two different isotopes the structure is chiral. There may therefore be three different chiral structures for both $CH_3D_2^+$ and $CH_2D_3^+$ (without counting the enantiomers).

Whether partial deuteration of CH_5^+ induces isomerism or not depends on the heights of the barriers and the differences in the vibrational zero-point corrections. The purely electronic barrier heights are known from accurate ab initio calculations[86] and are indicated in Figure 19. They are low compared to the case of CH_4^+ and therefore, the vibrational zero-point energy corrections are expected to become dominant. The calculations reported in Refs. [89–91] indicate that deuteration partially suppresses tunneling but the effect may be too small to induce an isomerism of the kind discussed above for the methane cation. Indeed, the vibrational wavefunctions may well have amplitude in minima corresponding to several distinct isomeric structures.

Partial deuteration could nevertheless facilitate the assignment of the infrared spectrum. First, the distinct stretching frequencies of the C–H and C–D chromophores will reduce spectral congestion. Moreover, the inequivalence of the different minima induced by different zero-point-energy corrections leads to a partial localization of the nuclear wavefunctions and therefore a higher rigidity of the molecule. In the case of the methane cation, the inspection of the PFI-ZEKE photoelectron spectra of $CH_2D_2^+$ and CH_3D^+ immediately reveals the existence of three and two isomers, respectively, which establishes the C_{2v} symmetry of the minimum energy structure.

7. Summary and Outlook

The theorem formulated by Jahn and Teller[3] namely that "*All non-linear nuclear configurations are unstable for an orbitally degenerate electronic state*" and reformulated by Jahn[4] "*A configuration of a polyatomic molecule for an electronic state having orbital degeneracy cannot be stable with respect to all displacements of the nuclei unless in the original configuration the nuclei all lie on a straight line*" does not contain explicit indications on the (equilibrium) nuclear configuration nor on the chemical reasons or the mechanisms for the spontaneous distortion of the nuclear framework. The manifestations of the theorem are much more diverse than the simplicity of the theorem suggests. As is often the case in molecular physics, each molecule represents a special case.

In molecules with a high degree of permutational symmetry, such as those considered in this Review, several equivalent distorted minimum-energy structures result from the Jahn–Teller effect, often connected by a network of tunneling paths and mechanisms. When the energy barriers separating the minimum-energy structures are low, the Jahn–Teller effect results in a high fluxionality of the molecule. The corresponding quantum-level structures are complex and cannot be measured, analyzed, or predicted with the standard methods used for rigid molecules. Experimentally, the use of double-resonance methods, which enable the transitions observed in a spectrum to be grouped according to the nuclear spin symmetry, greatly facilitate initial assignments.

Photoelectron spectroscopy offers distinct advantages for the study of molecular cations that are subject to the JT effect. Many vibrational states are accessible, particularly those associated with the JT active modes, and high-resolution methods, such as PFI-ZEKE photoelectron spectroscopy, give access to their rotational energy level structure. Theoretically, the point groups adequate for rigid molecules can no longer be used to classify the quantum levels and have to be replaced by the molecular symmetry groups.[22] The quantum-level structure resulting from the tunneling dynamics can be qualitatively predicted by correlating the point group of the distorted structure to the molecular symmetry group of the fluxional molecule. In conjunction with ab initio quantum chemical calculations, this methodology permits the prediction and classification of the complete rovibronic structure.

Isotopic substitutions are an essential tool in studies of the tunneling dynamics of highly symmetric molecules. They allow the permutational symmetry to be reduced and remove the energetic equivalence of potential-energy minima without affecting the nature of the electronic potential-energy surfaces. Isotopic substitution enables the zero-point energies of otherwise equivalent structures to be changed and allows the consequences of the reduced degree of degeneracy on the dynamics of the molecule to be investigated. In particular we have shown that it can suppress some tunneling paths at low energies, thereby inducing rigidity of the nuclear framework and giving rise to unusual forms of isomerism and chirality.

Herein we concentrated on two fundamental cations, the methane cation and the cyclopentadienyl cation, which are representative examples of the diversity of spectral, structural, and dynamic manifestations of the JT effect in highly symmetric molecules. The common aspect of the JT effect in both cations is that it leads to a partial localization of the electronic wavefunctions and to a delocalization of the nuclear wavefunctions over several equivalent configurations. We have determined how these molecular cations distort and have rationalized the distortions using chemical intuition. The methane cation distorts to a structure resembling a van der Waals complex of CH_2^+ and H_2, which can be attributed to the low ionization energy of CH_2 and the strength of the bond of H_2. The cyclopentadienyl cation in its lowest singlet state distorts to dienylic and allylic structures that permit the localization of electrons and avoid the delocalized antiaromatic structure.

In future, as theoretical and computational tools improve, the treatment of an increasing number of degrees of freedom will become possible using highly accurate ab initio quantum-chemical calculations and numerically exact computations of vibrational energy levels. Experimentally, the measurements of spectra at higher resolution would be desirable, particularly in view of observing spin–orbit and spin–rotational structures and, to date, unobserved tunneling splittings, which would allow an even more precise characterization of the nuclear

structure and dynamics. In particular, direct spectroscopic measurements in the microwave and IR ranges would ideally complement the information obtained by photoelectron spectroscopy.

The JT effect and its consequences on the rovibronic quantum-level structure and dynamics of larger highly symmetric molecules, such as symmetrically substituted transition metals or C_{60}^{+}, remain largely uncharacterized. Obtaining information on these systems constitutes an immense challenge, both theoretically and experimentally, and will hopefully continue to stimulate experimental and theoretical progress.

We thank Prof. M. Quack for his continued encouraging interest in our research and fruitful discussions. We thank Prof. R. Signorell, Dr. M. Sommavilla, R. van der Veen and Dr. X. Qian, Dr. A. M. Schulenburg, Prof. S. Willitsch and M. Grütter for their contributions to the work summarized in this review article. This work is supported financially by the Swiss National Science Foundation and the ETH Zürich.

Received: January 28, 2009

[1] I. B. Bersuker, *The Jahn–Teller Effect*, Cambridge University Press, Cambridge, **2006**.
[2] *Conical Intersections: Electronic Structure, Dynamics and Spectroscopy* (Eds.: W. Domcke, D. R. Yarkony, H. Köppel), World Scientific, Singapore, **2004** (*Adv. Ser. Phys. Chem.*, *Vol. 15*).
[3] H. A. Jahn, E. Teller, *Proc. R. Soc. London Ser. A* **1937**, *161*, 220.
[4] H. A. Jahn, *Proc. R. Soc. London Ser. A* **1938**, *164*, 117.
[5] H. C. Longuet-Higgins, U. Öpik, M. H. L. Pryce, R. A. Sack, *Proc. R. Soc. London Ser. A* **1958**, *244*, 1.
[6] H. C. Longuet-Higgins, *Advances in Spectroscopy*, *Vol. 2*, Interscience, New York, **1961**.
[7] I. B. Bersuker, *Sov. Phys. JETP* **1963**, *16*, 933.
[8] U. Öpik, M. H. L. Pryce, *Proc. R. Soc. London Ser. A* **1957**, *238*, 425.
[9] H. von Busch, V. Dev, H.-A. Eckel, S. Kasahara, J. Wang, W. Demtröder, P. Sebald, W. Meyer, *Phys. Rev. Lett.* **1998**, *81*, 4584; Erratum: H. von Busch, V. Dev, H.-A. Eckel, S. Kasahara, J. Wang, W. Demtröder, P. Sebald, W. Meyer, *Phys. Rev. Lett.* **1999**, *82*, 3560.
[10] R. Meiswinkel, H. Köppel, *Chem. Phys.* **1990**, *144*, 117.
[11] W. E. Ernst, S. Rakowsky, *Phys. Rev. Lett.* **1995**, *74*, 58.
[12] R. Lindner, K. Müller-Dethlefs, E. Wedum, K. Haber, E. R. Grant, *Science* **1996**, *271*, 1698.
[13] M. Ford, R. Lindner, K. Müller-Dethlefs, *Mol. Phys.* **2003**, *101*, 705.
[14] H. Köppel, L. S. Cederbaum, W. Domcke, S. S. Shaik, *Angew. Chem.* **1983**, *95*, 221; *Angew. Chem. Int. Ed. Engl.* **1983**, *22*, 210.
[15] H. Köppel, W. Domcke, L. S. Cederbaum, *Adv. Chem. Phys.* **1984**, *57*, 59.
[16] J. W. Zwanziger, E. R. Grant, *J. Chem. Phys.* **1987**, *87*, 2954.
[17] T. A. Barckholtz, T. A. Miller, *Int. Rev. Phys. Chem.* **1998**, *17*, 435.
[18] B. E. Applegate, T. A. Barckholtz, T. A. Miller, *Chem. Soc. Rev.* **2003**, *32*, 38.
[19] C. C. Chancey, M. C. M. O'Brien, *The Jahn–Teller Effect in C_{60} and Other Icosahedral Complexes*, Princeton University Press, Princeton, **1997**.
[20] K. Müller-Dethlefs, E. W. Schlag, *Annu. Rev. Phys. Chem.* **1991**, *42*, 109.
[21] K. Müller-Dethlefs, E. W. Schlag, *Angew. Chem.* **1998**, *110*, 1414; *Angew. Chem. Int. Ed.* **1998**, *37*, 1346.
[22] P. R. Bunker, P. Jensen, *Molecular Symmetry and Spectroscopy*, 2nd ed., NRC Research Press, Ottawa, **1998**.
[23] H. Köppel, L. S. Cederbaum, W. Domcke, *Chem. Phys. Lett.* **1984**, *110*, 469.
[24] I. B. Bersuker, V. Z. Polinger, *Sov. Phys. JETP* **1974**, *39*, 1023.
[25] A. Bohm, A. Mostafazadeh, H. Koizumi, Q. Niu, J. Zwanziger, *The Geometric Phase in Quantum Systems: Foundations, Mathematical Concepts and Applications in Molecular and Condensed Matter Physic*, Springer, Heidelberg, **2003**.
[26] J. K. Cullum, R. A. Willoughby, *Lanczos Algorithms for Large Symmetric Eigenvalue Computations*, Birkhauser, Boston, **1985**.
[27] M. J. Paterson, M. J. Bearpark, M. A. Robb, L. Blancafort, G. A. Worth, *Phys. Chem. Chem. Phys.* **2005**, *7*, 2100.
[28] G. Herzberg, H. C. Longuet-Higgins, *Discuss. Faraday Soc.* **1963**, *35*, 77.
[29] H. J. Wörner, R. van der Veen, F. Merkt, *Phys. Rev. Lett.* **2006**, *97*, 173003.
[30] W. T. Borden, *Diradicals*, Wiley, New York, **1982**.
[31] H. Köppel, L. S. Cederbaum, W. Domcke, *J. Chem. Phys.* **1988**, *89*, 2023.
[32] J. K. G. Watson, *Mol. Phys.* **1999**, *96*, 1721.
[33] W. T. Borden, E. R. Davidson, *J. Am. Chem. Soc.* **1979**, *101*, 3771.
[34] H. J. Wörner, F. Merkt, *J. Chem. Phys.* **2007**, *127*, 034303.
[35] M. N. Paddon-Row, D. J. Fox, J. A. Pople, K. N. Houk, D. W. Pratt, *J. Am. Chem. Soc.* **1985**, *107*, 7696.
[36] R. F. Frey, E. R. Davidson, *J. Chem. Phys.* **1988**, *88*, 1775.
[37] R. Signorell, F. Merkt, *Faraday Discuss.* **2000**, *115*, 205.
[38] M. Quack, *Angew. Chem.* **1989**, *101*, 588; *Angew. Chem. Int. Ed. Engl.* **1989**, *28*, 571.
[39] M. Quack, J. Stohner, M. Willeke, *Annu. Rev. Phys. Chem.* **2008**, *59*, 741.
[40] M. S. Reeves, E. R. Davidson, *J. Chem. Phys.* **1991**, *95*, 6551.
[41] H. J. Wörner, X. Qian, F. Merkt, *J. Chem. Phys.* **2007**, *126*, 144305.
[42] G. Herzberg, *Molecular Spectra and Molecular Structure*, *Vol. II*, *Infrared and Raman Spectra of Polyatomic Molecules*, Krieger, Malabar, **1991**.
[43] F. Merkt, *Annu. Rev. Phys. Chem.* **1997**, *48*, 675.
[44] E. W. Schlag, *ZEKE Spectroscopy*, Cambridge University Press, Cambridge, **1998**.
[45] U. Hollenstein, R. Seiler, H. Schmutz, M. Andrist, F. Merkt, *J. Chem. Phys.* **2001**, *115*, 5461.
[46] D. E. Cooper, C. M. Klimack, J. E. Wessels, *Phys. Rev. Lett.* **1981**, *46*, 324.
[47] B. Bobin, *J. Phys.* **1972**, *33*, 345.
[48] S. Willitsch, J. M. Dyke, F. Merkt, *Helv. Chim. Acta* **2003**, *86*, 1152.
[49] H. J. Wörner, F. Merkt, *Angew. Chem.* **2006**, *118*, 299; *Angew. Chem. Int. Ed.* **2006**, *45*, 293.
[50] M. Saunders, R. Berger, A. Jaffe, J. M. McBride, J. O'Neill, R. Breslow, J. M. Hoffmann, C. Perchonock, E. Wassermann, R. S. Hutton, V. J. Kuck, *J. Am. Chem. Soc.* **1973**, *95*, 3017.
[51] T. Bally, S. Masamune, *Tetrahedron* **1980**, *36*, 343.
[52] G. Maier, *Angew. Chem.* **1988**, *100*, 317; *Angew. Chem. Int. Ed. Engl.* **1988**, *27*, 309.
[53] R. Signorell, F. Merkt, *J. Chem. Phys.* **1999**, *110*, 2309.
[54] M. Quack, *Mol. Phys.* **1977**, *34*, 477.
[55] M. Hippler, M. Quack, *Chem. Phys. Lett.* **1999**, *314*, 273.
[56] S. Willitsch, L. L. Imbach, F. Merkt, *J. Chem. Phys.* **2002**, *117*, 1939.
[57] A. Carrington, H. Longuet-Higgins, R. Moss, P. Todd, *Mol. Phys.* **1965**, *9*, 187.
[58] R. G. Lawler, J. R. Bolton, G. K. Fraenkel, T. H. Brown, *J. Am. Chem. Soc.* **1964**, *86*, 520.

[59] B. Scharf, R. Vitenberg, B. Katz, Y. B. Band, *J. Chem. Phys.* **1982**, *77*, 2226.
[60] L. Yu, D. W. Cullin, J. M. Williamson, T. A. Miller, *J. Chem. Phys.* **1993**, *98*, 2682.
[61] H. J. Wörner, F. Merkt, *J. Chem. Phys.* **2007**, *126*, 154304.
[62] R. Signorell, M. Sommavilla, F. Merkt, *Chem. Phys. Lett.* **1999**, *312*, 139.
[63] M. Quack, *Nova Acta Leopold.* **1999**, *81*, 1.
[64] R. Berger, G. Laubender, M. Quack, A. Sieben, J. Stohner, M. Willeke, *Angew. Chem.* **2005**, *117*, 3689; *Angew. Chem. Int. Ed.* **2005**, *44*, 3623.
[65] L. Wang, J. E. Pollard, Y. T. Lee, D. A. Shirley, *J. Chem. Phys.* **1987**, *86*, 3216.
[66] S. Willitsch, U. Hollenstein, F. Merkt, *J. Chem. Phys.* **2004**, *120*, 1761.
[67] A. M. Schulenburg, Diss. ETH Nr. 18024, Dissertation, Eidgenössische Technische Hochschule ETH Zürich, **2008**.
[68] B. Fehrensen, D. Luckhaus, M. Quack, *Chem. Phys. Lett.* **1999**, *300*, 312.
[69] M. Gottselig, D. Luckhaus, M. Quack, J. Stohner, M. Willeke, *Helv. Chim. Acta* **2001**, *84*, 1846.
[70] R. Berger, M. Gottselig, M. Quack, M. Willeke, *Angew. Chem.* **2001**, *113*, 4342; *Angew. Chem. Int. Ed.* **2001**, *40*, 4195.
[71] M. Gottselig, M. Quack, *J. Chem. Phys.* **2005**, *123*, 084305.
[72] M. J. M. Pepper, I. Shavitt, P. v. R. Schleyer, M. N. Glukhovtsev, R. Janoschek, M. Quack, *J. Comput. Chem.* **1995**, *16*, 207.
[73] M. J. Frisch, G. W. Trucks, H. B. Schlegel, G. E. Scuseria, M. A. Robb, J. R. Cheeseman, J. A. Montgomery, Jr., T. Vreven, K. N. Kudin, J. C. Burant, J. M. Millam, S. S. Iyengar, J. Tomasi, V. Barone, B. Mennucci, M. Cossi, G. Scalmani, N. Rega, G. A. Petersson, H. Nakatsuji, M. Hada, M. Ehara, K. Toyota, R. Fukuda, J. Hasegawa, M. Ishida, T. Nakajima, Y. Honda, O. Kitao, H. Nakai, M. Klene, X. Li, J. E. Knox, H. P. Hratchian, J. B. Cross, V. Bakken, C. Adamo, J. Jaramillo, R. Gomperts, R. E. Stratmann, O. Yazyev, A. J. Austin, R. Cammi, C. Pomelli, J. W. Ochterski, P. Y. Ayala, K. Morokuma, G. A. Voth, P. Salvador, J. J. Dannenberg, V. G. Zakrzewski, S. Dapprich, A. D. Daniels, M. C. Strain, O. Farkas, D. K. Malick, A. D. Rabuck, K. Raghavachari, J. B. Foresman, J. V. Ortiz, Q. Cui, A. G. Baboul, S. Clifford, J. Cioslowski, B. B. Stefanov, G. Liu, A. Liashenko, P. Piskorz, I. Komaromi, R. L. Martin, D. J. Fox, T. Keith, M. A. Al-Laham, C. Y. Peng, A. Nanayakkara, M. Challacombe, P. M. W. Gill, B. Johnson, W. Chen, M. W. Wong, C. Gonzalez, J. A. Pople. Gaussian 03, Revision C.02. Gaussian, Inc., Wallingford, CT, 2004.
[74] A. Garg, *Am. J. Phys.* **2000**, *68*, 430.
[75] J. T. Hougen in *Methane Symmetry Operation*, *MTP International Reviews of Science*, *Physical Chemistry*, *Vol. 3* (Eds.: D. A. Ramsay), Butterworth, London, **1976**.
[76] A. Olah, G. Rasul, *Acc. Chem. Res.* **1997**, *30*, 245.
[77] E. Herbst, *J. Phys. Chem. A* **2005**, *109*, 4017.
[78] E. T. White, J. Tang, T. Oka, *Science* **1999**, *284*, 135.
[79] O. Asvany, P. Kumar, B. Redlich, I. Hegemann, S. Schlemmer, D. Marx, *Science* **2005**, *309*, 1219.
[80] X. Huang, A. B. McCoy, J. M. Bowman, L. M. Johnson, C. Savage, F. Dong, D. J. Nesbitt, *Science* **2006**, *311*, 60.
[81] X.-G. Wang, T. Carrington, Jr., *J. Chem. Phys.* **2008**, *129*, 234102.
[82] A. Komornicki, D. A. Dixon, *J. Chem. Phys.* **1987**, *86*, 5625.
[83] W. Klopper, W. Kutzelnigg, *J. Phys. Chem.* **1990**, *94*, 5625.
[84] P. R. Schreiner, S.-J. Kim, H. F. Schafer III, P. v. R. Schleyer, *J. Chem. Phys.* **1993**, *99*, 3716.
[85] P. R. Schreiner, *Angew. Chem.* **2000**, *112*, 3375; *Angew. Chem. Int. Ed.* **2000**, *39*, 3239.
[86] A. Brown, A. B. McCoy, B. J. Braams, Z. Jin, J. M. Bowman, *J. Chem. Phys.* **2004**, *121*, 4105.
[87] Z. Jin, B. J. Braams, J. M. Bowman, *J. Phys. Chem. A* **2006**, *110*, 1569.
[88] P. R. Bunker, B. Ostojić, S. Yurchenko, *J. Mol. Struct.* **2004**, *695–696*, 253.
[89] A. B. McCoy, B. J. Braams, A. Brown, X. Huang, Z. Jin, J. M. Bowman, *J. Phys. Chem. A* **2004**, *108*, 4991.
[90] L. M. Johnson, A. B. McCoy, *J. Phys. Chem. A* **2006**, *110*, 8213.
[91] X. Huang, L. M. Johnson, J. M. Bowman, A. B. McCoy, *J. Am. Chem. Soc.* **2006**, *128*, 3478.

